



OPEN

Bayat-driven FOPIID controller design for biogas-based microgrid with real-time validation

T. K. Bashishtha¹, V. P. Singh¹, Tarun Varshney² & Sanjeevikumar Padmanaban³✉

The energy policies of the 21st century are increasingly focused on promoting generation solutions with minimal environmental impact. In response to strategic initiatives, the accelerating depletion of fossil fuel reserves has led to integrating renewable sources for power generation. The uncertain nature of solar and wind energy sources, along with fluctuating load demands, leads to frequency instability. This study addresses the challenge of frequency instability by designing a Bayat-tuned fractional-order proportional-integral-derivative (FOPIID) controller for a decentralized microgrid ($Dz\mu G$). The proposed $Dz\mu G$ model consists of environmentally friendly energy sources such as a biogas turbine generator (BTG), a biodiesel engine generator (BEG), other distributed generation units (DGUs), and energy storage devices (ESDs). The mathematical modeling of $Dz\mu G$ components is carried out using first-order transfer functions, which are combined to derive the overall transfer function of $Dz\mu G$ model. This composite model is then approximated as a first-order plus time delay (FOPTD) system to simplify FOPIID controller design. The parameters of the FOPIID controller are optimized using the Bayat method to achieve robust performance under set-point tracking (SPT) and load disturbance rejection (LDR) scenarios. Based on this approach, three controller variants i.e., FOPIID-*Bayat*_{SP1.4}, FOPIID-*Bayat*_{SP2.0}, and FOPIID-*Bayat*_{LD1.4}, are developed. To validate the effectiveness of the proposed control strategy, various simulation scenarios are considered, including load disturbances and varying levels of solar and wind power penetration. The performance of the controllers is evaluated in terms of frequency deviation, error mitigation, and transient behavior under SPT and LDR conditions. A comparative analysis using error indices, time-domain metrics, control effort, and frequency plots confirms the effectiveness of the Bayat-tuned FOPIID designs. Furthermore, real-time validation using the OPAL-RT simulator underscores their practical potential in maintaining frequency stability within $Dz\mu G$ systems. Owing to the performance analysis, it is justified that discussed FOPIID-*Bayat* controllers consistently ensured controllability with a minimum rise time of 4.02×10^{-5} s, a nearly constant settling time of ~ 49.8 s, and reduced control effort down to 0.12. Furthermore, error index evaluation confirmed that FOPIID-*Bayat*_{SP2.0} outperformed other configurations by achieving the lowest IAE (8.737), ITAE (223.0), ITSE (40.39), and ISE (1.706), thereby demonstrating superior efficiency and robustness.

Keywords Fractional Order PID, Bayat method, Decentralized Microgrid, Biogas Generator, Real-Time Simulation, Frequency Control

Abbreviations

$Dz\mu G$	Decentralized microgrid
BEG	Biodiesel engine generator
BTG	Biogas turbine generator
BESS	Battery energy storage system
DGUs	Distributed generation units
DEG	Diesel engine generator
ESDs	Energy storage devices
EVs	Electric vehicles
FESS	Flywheel energy storage system

¹Dept. of Electrical Engineering, Malaviya National Institute of Technology, Jaipur 302017, Rajasthan, India.

²Dept. of EECE, SSES, Sharda University, Greater Noida, UP, India. ³Department of Electrical Engineering, IT and Cybernetics, University of South-Eastern Norway, Porsgrunn, Norway. ✉email: sanjeevi_12@yahoo.co.in

FOPTD	First-order plus time delay
FOPID	Fractional order proportional-integral-derivative
LDR	Load disturbance rejection
LFC	Load frequency control
MTG	Microturbine generator
RESs	Renewable energy sources
SPT	Set-point tracking
SPV	Solar photovoltaic
UC	Ultracapacitor
WTG	Wind-turbine generator

List of symbols

M	Inertia constant
D	Damping constant
$FOPID$ -Bayat _{SP1.4}	FOPID for 1.4 SPT
$FOPID$ -Bayat _{SP2.0}	FOPID for 2.0 SPT
$FOPID$ -Bayat _{LDR1.4}	FOPID for 1.4 LDR
G_{sys}	Transfer function of dynamics
G_{con}	Transfer function of controllable sources
G_{ESD}	Transfer function of ESD
G_{inner}	Transfer function of inner loop
C_{FOPID} -Bayat _{SP1.4}	Controller for SP1.4
C_{FOPID} -Bayat _{SP2.0}	Controller for SP2.0
C_{FOPID} -Bayat _{LDR1.4}	Controller for LDR1.4
$G_{Dz\mu G}$	Transfer function of decentralized microgrid
P_{error}	Net power error
P_L	Load power
Δf	Frequency deviation
P_{PV}, P_{WT}	Powers of PV and WT
K, T_d, T_m	FOPTD parameters
$P_{BESS}, P_{FESS}, P_{UC}, P_{EV}$	Power of BESS, FESS, UC, EV
$P_{DG}, P_{MT}, P_{BEG}, P_{BTG}$	Powers of DG, MT, BEG, BTG

Motivation and background

In the 21st century, energy policies increasingly prioritize sustainable generation methods that minimize environmental impact¹. This shift is driven by the dual pressures of strategic energy planning and the accelerating depletion of fossil fuel resources, both of which have significantly increased global interest in renewable energy sources (RESs) as alternatives to conventional power generation². Traditional energy systems face several inherent challenges, including high levels of pollution, complex and rigid network infrastructures, and economic inefficiencies due to considerable transmission and distribution losses. These drawbacks have catalyzed the development of microgrids as a more adaptable and sustainable solution.

Microgrids, particularly in remote or off-grid regions, offer a practical and cost-effective alternative where extending the main grid is neither feasible nor economical. By integrating RESs, microgrids address the limitations of conventional systems while offering several operational advantages such as reduced transmission losses, improved system reliability and security, enhanced scalability, and more flexible control architectures. Furthermore, the use of RESs significantly reduces the environmental footprint of power generation, helping to mitigate the negative effects associated with fossil fuel consumption³. Beyond environmental benefits, RES integration also presents opportunities for significant cost savings and improved energy resilience, making microgrids a promising component of modern energy systems.

Literature on microgrid models

A decentralized microgrid ($Dz\mu G$) typically comprises both controlled and uncontrolled sources, spanning conventional and renewable technologies, along with energy storage systems and dynamic loads⁴. The primary objective of a $Dz\mu G$ is to coordinate and optimize the operation of its diverse generation units and storage systems to reliably meet continuously fluctuating load demands⁵. In response to rising energy demands and growing environmental and economic concerns, there is a notable trend toward integrating more renewable (non-conventional) sources in place of conventional ones.

As per literature⁸, solar photovoltaic (SPV) systems and wind turbine generator (WTG) serve as typical uncontrolled renewable sources, while battery energy storage systems (BESS) and flywheel energy storage systems (FESS) are widely used to store surplus power. Diesel engine generator (DEG), on the other hand, are commonly employed as controlled sources to compensate for power deficits²⁶. Some models also incorporate thermal power plants alongside SPV, WTG, BESS, and FESS to diversify generation options^{7,8}.

Several microgrid configurations have been proposed in the literature^{27–29}, showcasing different combinations of controlled sources and storage devices. In more advanced architectures, fuel cells (FCs) are integrated with SPV, WTG, DEG, BESS, and FESS, serving as controllable units capable of utilizing surplus renewable energy via aqua-electrolyzers to produce hydrogen for later use^{10,30,31}. Other models explore the use of aqua-based fuels for power generation, supplementing traditional RESs and storage devices with components such as microturbine generators (MTGs) and DEGs to enhance system robustness^{9,10,12,32,33}. MTGs are particularly valuable for frequency regulation and improving power supply stability^{28,34}. Furthermore, electric vehicles (EVs) are gaining

attention as mobile energy storage units that can dynamically adjust their charging and discharging patterns in response to real-time load fluctuations³⁴.

The literature suggested that most of the researchers considered SPV, WTG, as uncontrollable sources, DEG, and MTG as controllable sources, and BESS, FESS for storage purposes. As per the author's knowledge, biogas turbine generator (BTG) and biodiesel engine generator (BEG) are not utilized as controllable units with SPV, WTG, DEG, MTG, BESS, FESS, EV for frequency stability of $Dz\mu G$. Integrating BTG and DEG in $Dz\mu G$ enhanced its reliability and made the environment eco-friendly, as these power generation units uses waste products for power generation. This is one of the main contributions of this article.

Despite the growing interest in decentralized microgrid systems, ensuring frequency stability under dynamic conditions remains a critical challenge, particularly in the presence of load disturbances and renewable energy intermittencies. The frequency stability of $Dz\mu G$ are maintained by keeping a proper balance between generation and load. As load and power generation through renewable sources are variable, it leads to the issue of load frequency control (LFC). LFC is managed with the help of storage units and additional controlled sources of conventional and non-conventional nature³⁵. To regulate power of controlled sources, various control schemes such as PD-PI¹¹ IPD-(1+I)⁶, PD-(1+PI)¹⁴, fuzzy PIDF³⁶, fuzzy PI-PD³⁷, type II fuzzy³⁸ and PID^{39,40}, FOPI⁴¹ are incorporated into $Dz\mu G$ as secondary control schemes to manage LFC. The detailed summary of microgrid schema with their control design is provided in Table 1. Conventional PID controllers often fall short in handling the complex dynamics and uncertainties inherent in such systems. Modified controllers are discussed in the literature^{34,42,43}. Sahu et. al in⁴³ presented an efficient control technique for an islanded microgrid of two area. Authors have designed type-II fuzzy based PID controller to maintain the tie-line power and frequency within the limits by incorporating various uncertainties. For optimal tuning of gain of PID controller, improved salp swarm optimization as an powerful algorithm has been implemented. Authors have also performed the comparative analysis for the designed controller with type-I fuzzy controller while outcomes of optimization algorithm have been compared with other popular algorithms. Furthermore, a fractional order PI controller is implemented by Sahu et al. in³⁴, by utilizing type2 fuzzy approach for maintaining the power flow as well as frequency of a complex multi-area microgrid considering various disturbances. Authors have used cow search algorithm for the optimum tuning of the controller parameters. In addition to that authors have performed comparative study validate the superiority of designed controller over generalised type-2, PID based on fuzzy type-1 and PID controllers.

Moreover, the issue related with the frequency fluctuation in a renewable and EV integrated microgrid architecture, is taken into account⁴⁴. Author has developed a fractional order control scheme as power system stabilizer based on fuzzy technique tuned with advanced sine cosine algorithm for reducing the duration of settling time of frequency deviation. In addition to the approaches in the segment of regulating the frequency, Bhatta et. al in⁴⁵ have proposed a fractional order based controller utilizing type 2 fuzzy technique to frequency and voltage profile of two area microgrid facilitated with various renewable integration having different uncertainties. In the aforementioned approach, author has exploited an algorithm based on Quassi- oppositional path finderfor the optimum selection of controller parameters.

Ref.	Renewable sources	Controllable sources	Controller	BESS	FESS	Other storage
6	SPV, WTG	MT, FC, DEG	IPD-(1+I)	✓	✓	✗
7	SPV, WTG	Thermal	PI	✗	✗	✗
8	SPV, WTG	Thermal unit	Fuzzy-PID	✓	✓	✗
9	WTG, SPV	DEG, MTG, FC	PID	✓	✓	✗
10	SPV, WTG	FC, DEG, MT	Multi-stage PID	✓	✓	✗
11	SPV, WTG	DEG, FC	PD-PI	✓	✗	PEV
12	SPV, WTG	AE-FC, DEG	PD-PI	✓	✓	✗
13	SPV, WTG	BEG, BTG	Fuzzy-PID	✓	✓	✗
14	WTG, SPV	FC, DEG	PD-(1+PI)	✓	✗	✗
15	SPV, WTG	MT, FC, DEG	PID	✓	✓	✗
16	SPV	BEG, BTG	I, PI, PD, PID, PIDF	✓	✗	✗
17	SPV, SWE	BGT, PEMFC	PI(1+PD)	✓	✓	SMES
18	SPV, WTG	AE-FC, DEG, MT	PID	✓	✓	✗
19	SPV, WTG	AE-FC, DEG, MT	PI	✓	✓	UC
20	SPV, WTG	AE-FC	fuzzy PID	✗	✗	UC, EV
21	SPV, WTG	DEG	PD-PI	✗	✗	PHEV
22	SPV, WTG	-	PID	✓	✗	✗
23	SPV, WTG	BGT, BEG, Hydro	PI, PID, PIDF	✓	✗	✗
24	SPV, WTG	DEG	2-DOF-PID	✓	✓	EV
25	SPV, WTG	DEG	Fuzzy-PI	✓	✗	✗
Proposed	SPV, WTG	DEG, MTG, BEG, BTG	FOPID	✓	✓	UC, EV

Table 1. Literature available on $Dz\mu G$ architecture and controller.

Fractional-order PID (FOPID) controllers effectively deal with complex dynamics and system uncertainty, and offer enhanced flexibility with improved performance. In literature, there is a lack of comprehensive studies applying systematic tuning methods such as the Bayat method to FOPID controllers for decentralized microgrids. Moreover, the suitability of different Bayat tuning configurations for specific control objectives like set-point tracking and load disturbance rejection remains underexplored.

This research is motivated by the need to fill this gap by investigating the application of the Bayat tuning method for designing FOPID controllers tailored to a $Dz\mu G$ model. This study aims to develop an effective control strategy that not only stabilizes frequency but also optimizes transient performance and control effort for a $Dz\mu G$ model.

A key contribution of this work lies in the novel integration of Bayat methodology-based tuning, First Order Plus Time Delay (FOPTD) system modeling, and real-time validation, which has not been explored previously in the context of microgrid frequency regulation. While each of these elements has been studied independently in prior research, their combined application offers a comprehensive framework that bridges theoretical controller design and practical implementation. This synergistic approach enhances the robustness and reliability of fractional-order PID (FOPID) controllers under dynamic operating conditions, demonstrating a clear advancement in the field of intelligent control for renewable-integrated microgrids.

Contribution and highlights of study

The major contribution of this article is the investigation of Bayat assisted FOPID controller for enhancing frequency stability of $Dz\mu G$ model. However, our contribution lies in applying Bayat method under set-point and load disturbance scenarios to design an FOPID controller that can maintain the frequency stability of a biogas-based $Dz\mu G$. The FOPID controller efficacy in managing the frequency stability is validated through OPAL-RT. To implement FOPID controller, the linear transfer function of the $Dz\mu G$ model is derived by linearizing and approximating the system as a first-order plus time delay (FOPTD) model. The FOPID controller is then designed for both set-point tracking and load disturbance rejection modes. A comparative analysis of various FOPID controller variants including FOPID- $Bayat_{SP1.4}$, FOPID- $Bayat_{SP2.0}$, and FOPID- $Bayat_{LD1.4}$ is conducted to determine the most effective control design for maintaining frequency stability of $Dz\mu G$. The effectiveness of this tuning method is validated through detailed evaluations of transient responses, control signal magnitudes, and frequency deviation profiles under SPT, LDR and variations in load, solar and wind power. Furthermore, the presented tabulated data of parametric sensitivity and real time validation support the robustness and suitability of the FOPID control designs for achieving frequency stability of $Dz\mu G$. The significant contributions of the presented article are summarized as follows:

- Developed a novel architecture for decentralized Microgrid ($Dz\mu G$) incorporating eco-friendly generation sources, including a biogas turbine generator and a biodiesel engine generator, along with other Distributed Generation Units (DGUs) and Energy Storage Devices (ESDs).
- Designed a fractional order proportional-integral-derivative (FOPID) controller to manage frequency deviations and frequency stability of $Dz\mu G$, utilizing a first-order model-based mathematical representation of the $Dz\mu G$.
- Implemented the Bayat method for both set point tracking and load disturbance rejection scenarios to determine FOPID controller parameters, aiming to maintain frequency stability of $Dz\mu G$ model.
- Ensured robustness of the FOPID controller for frequency regulation by performing parametric sensitivity analysis.
- Evaluated the performance of the various variations of the FOPID controller to maintain frequency stability during multiple load variations, and variations in solar and wind power, focusing on frequency error mitigation, with minimal controller effort, and attaining a feasible transient response.
- Validated the effectiveness of FOPID controllers i.e., FOPID- $Bayat_{SP1.4}$, FOPID- $Bayat_{SP2.0}$, and FOPID- $Bayat_{LD1.4}$, through real-time simulation using the OPAL-RT platform, demonstrating successful frequency error mitigation for the $Dz\mu G$ model.

Organization of the study

The outline of this article is structured as follows. Section II deals with architecture and equivalent modeling of decentralized Microgrid ($Dz\mu G$). Further, approximation based modelling of $Dz\mu G$ is discussed in section III. Section IV contains FOPID controller design approach and Bayat tuning method. Section V presents results and discussion utilizing Bayat tuning method under SPT and LDR scenarios. Various analyses and main findings are also provided in this section. Further, the concluding remarks with future directions are presented in section VI.

System under study: decentralized microgrid

The generalized schema of a decentralized microgrid ($Dz\mu G$) is shown in Fig. 1. The presented model is categorized into three categories, i.e., renewable energy sources, controllable sources, and energy storage devices. In Fig. 1, PV and WTG are renewable energy sources, and DEG, BEG, BTG, and MTG are controllable sources. Moreover, BESS, FESS, UC, and EV are considered as storage units. The main aim of these components is to meet the load demand of the connected load. In Fig. 1 all components are equipped with various power electronic based converters to convert power from AC to DC and vice-versa.

The block diagram illustrating microgrid model in Fig. 1 is further elaborated into closed loop based modelling of microgrid components, which are depicted in Fig. 2. It consists system dynamics (G_{sys}), controllable sources (G_{con}), energy storage devices (G_{ESD}), and a unity feedback. The mathematical expression for G_{sys} , G_{ESD} and G_{con} can be expressed in (1)-(3). These models are further classified into two control loops, i.e., primary and secondary loops. G_{sys} and G_{ESD} are main components of primary loop and form a inner closed

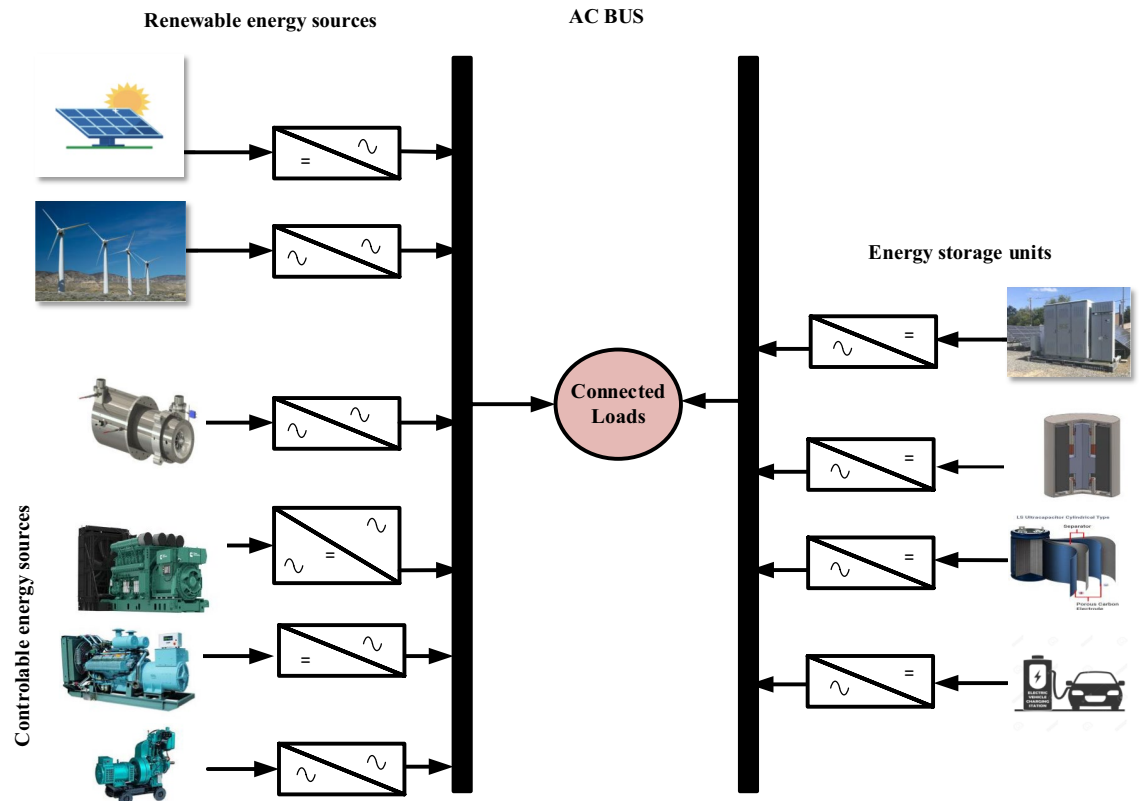


Fig. 1. Schema of decentralized microgrid.

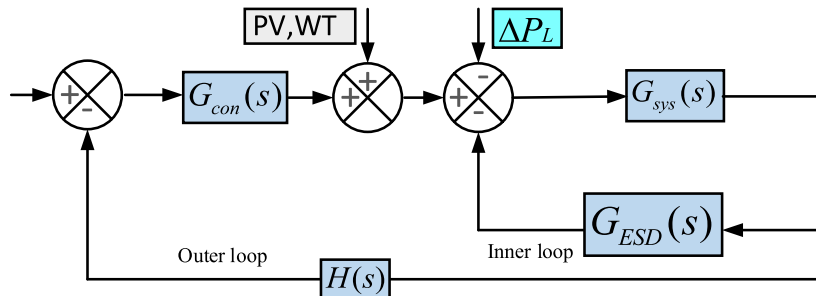


Fig. 2. Closed loop based modelling of $Dz\mu G$ components.

loop, which is expressed as G_{inner} , where as G_{con} is the forward path gain, which is the integral part of secondary loop and connected in series with G_{inner} .

$$G_{con} = \frac{K_{DEG}}{1 + sT_{DEG}} + \frac{K_{BEG}}{1 + sT_{BEG}} + \frac{K_{BTG}}{1 + sT_{BTG}} + \frac{K_{MTG}}{1 + sT_{MTG}} \quad (1)$$

$$G_{ESD} = \frac{K_{BESS}}{1 + sT_{BESS}} + \frac{K_{FESS}}{1 + sT_{FESS}} + \frac{K_{UC}}{1 + sT_{UC}} + \frac{K_{EV}}{1 + sT_{EV}} \quad (2)$$

$$G_{sys} = \frac{1}{D + Ms} \quad (3)$$

A detailed analysis to obtain an equivalent transfer function is as follows.

$$G_{inner}(s) = \frac{G_{sys}(s)}{1 + G_{sys}(s)G_{ESD}(s)} \quad (4)$$

Considering the feedback path as unity, an equivalent model of $Dz\mu G$ i.e. $\hat{G}_{Dz\mu G}(s)$ is formed.

$$G_{Dz\mu G}(s) = \frac{G_{inner}(s)G_{con}(s)}{1 + G_{inner}(s)G_{con}(s)H(s)} \quad (5)$$

Utilizing the (4) and (5), the obtained equivalent transfer function of $Dz\mu G$ model is expressed in (6).

$$G_{Dz\mu G}(s) = \frac{0.06949s^7 + 1.699s^6 + 13.66s^5 + 42.05s^4 + 62.96s^3 + 49.31s^2 + 19.38s + 3.003}{0.008791s^9 + 0.2272s^8 + 2.053s^7 + 8.348s^6 + 20.52s^5 + 33.9s^4 + 36.97s^3 + 24.66s^2 + 8.909s + 1.318} \quad (6)$$

The closed loop based modelling of $Dz\mu G$ depicted in Fig. 2 is further simplified in Fig. 3 with a perspective of equivalent transfer function of DGUs and ESDs. It is categorized into four major categories as system dynamics (G_{sys}), energy storage devices (G_{ESD}), controllable sources (G_{con}), and power variations (ΔP_{PV} , ΔP_W). In Fig 3 primary control loop comprises ESDs, while the secondary control loop comprises controllable DGUs. Moreover, SPV and WTG plants with interconnected loads, are considered system-dependent components or disturbances due to power variations. The primary control mechanism involves ESDs for power adjustments, while the secondary control mechanism utilizes controllable DGUs to manage varying load demands⁴⁶. The mathematical formulations of DGUs and ESDs in transfer function form with the nominal value of associated variables with system dynamics are depicted in Table 2.

Figure 3 provides power exchange among various components of the presented model. $\Delta P_{sources}$ is the power produced by controllable sources, ΔP_{ESD} is the amount of exchangeable power of energy storage devices and ΔP_{PV} , ΔP_W are power produced by PV and WTG units. Frequency deviations (Δf) occurs due to deviations in P_{error} , which can be expresses as

$$\Delta f = \frac{1}{D + Ms} P_{error} \quad (7)$$

$$P_{error} = \Delta P_{sources} + \Delta P_{ESD} - P_L \quad (8)$$

where,

$$\Delta P_{sources} = \Delta P_{DEG} + \Delta P_{MTG} + \Delta P_{BEG} + \Delta P_{BTG} \quad (9)$$

$$P_{ESD} = \pm \Delta P_{BESS} \pm \Delta P_{FESS} \pm \Delta P_{UC} \pm \Delta P_{EV} \quad (10)$$

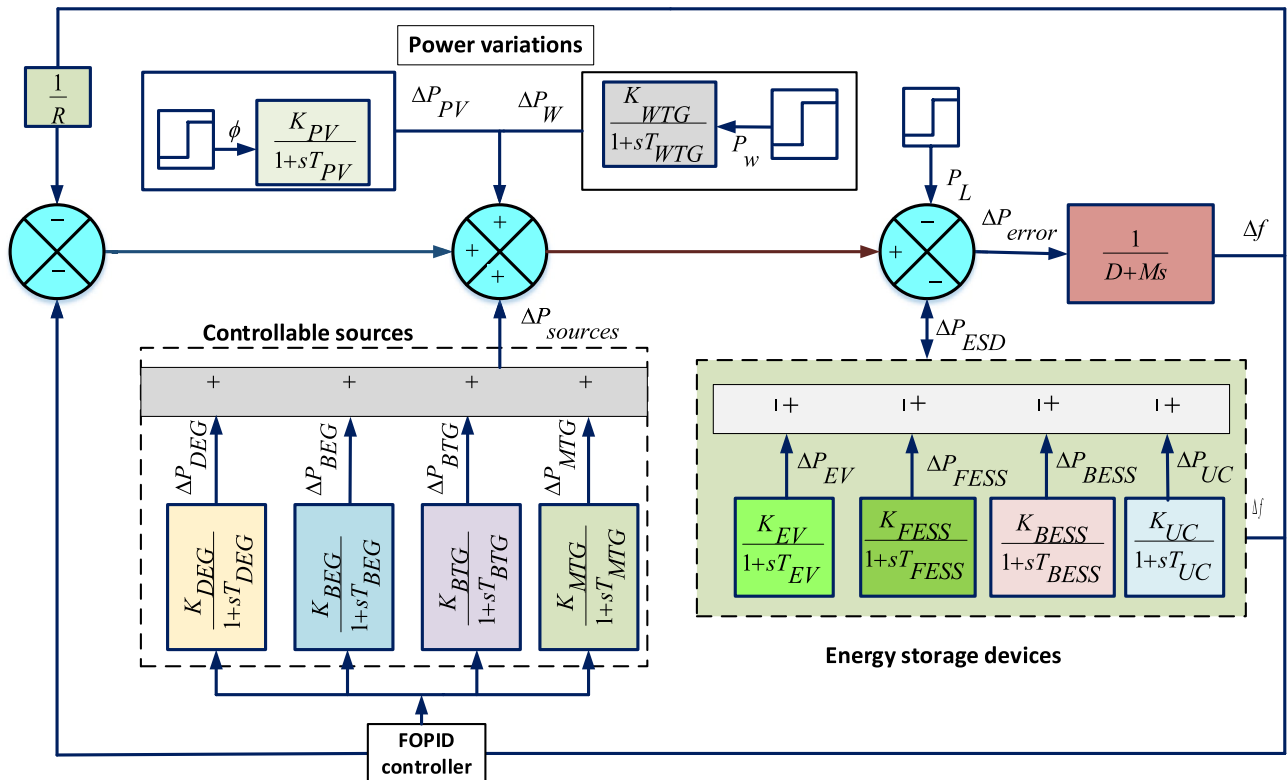


Fig. 3. Transfer function model.

Distributed Generating Units (DGUs)		
Component	Transfer Function	Parameters
Solar photovoltaic (SPV) ⁴⁷	$TF_{PV}(s) = \frac{K_{PV}}{1+sT_{PV}}$	$K_{PV} = 1, T_{PV} = 1.8$
Wind turbine generator (WTG) ⁴⁷	$TF_{WTG}(s) = \frac{K_{WTG}}{1+sT_{WTG}}$	$K_{WTG} = 1, T_{WTG} = 1.5$
Microturbine generator (MTG) ⁴⁷	$TF_{MTG}(s) = \frac{K_{MTG}}{1+sT_{MTG}}$	$K_{MTG} = 1, T_{MTG} = 1.5$
Biodiesel engine generator (BEG) ²³	$TF_{BEG}(s) \approx \frac{K_{BEG}}{1+sT_{BEG}}$	$K_{BEG} = 1, T_{BEG} = 0.55$
Biogas turbine generator (BTG) ²³	$TF_{BTG}(s) \approx \frac{K_{BTG}}{1+sT_{BTG}}$	$K_{BTG} = 1, T_{BTG} = 1.48$
Diesel engine generator (DEG) ⁴⁷	$TF_{DEG}(s) = \frac{K_{DEG}}{1+sT_{DEG}}$	$K_{DEG} = 0.003, T_{DEG} = 2$
Battery energy storage system (BESS) ⁴⁷	$TF_{BESS}(s) = \frac{K_{BESS}}{1+sT_{BESS}}$	$K_{BESS} = -0.003, T_{BESS} = 0.1$
Flywheel energy storage system (FESS) ⁴⁷	$TF_{FESS}(s) = \frac{K_{FESS}}{1+sT_{FESS}}$	$K_{FESS} = -0.01, T_{FESS} = 0.1$
Ultracapacitor (UC) ⁴⁸	$TF_{UC}(s) = \frac{K_{UC}}{1+sT_{UC}}$	$K_{UC} = -0.7, T_{UC} = 0.9$
Electric vehicle (EV) ⁴⁷	$TF_{EV}(s) \approx \frac{K_{EV}}{1+sT_{EV}}$	$K_{EV} = 1, T_{EV} = 1$
Inertia and damping ⁴⁷	$TF_{Dz\mu G}(s) = \frac{1}{D+sM}$	$D = 0.03, M = 0.4$

Table 2. Transfer Function of components of $Dz\mu$ with their values⁴⁶.

K	T_m	T_d
9.4993	2.2833	0.3951

Table 3. Parameters of FOPTD model⁴⁶.

Δf , shown in (78) can be minimized by managing P_{error} . Load demand (P_L) is supplied with the help of $\Delta P_{\text{sources}}$ and ΔP_{ESD} . In load frequency control ΔP_{PV} and ΔP_W are the power generated by solar and wind power plants, which is utilized in maximum capacity to meet load demand. These powers are stochastic in nature, which initiates a mismatch in power, leading to deviations in frequency. This is the main reason not to include these units in frequency control of the microgrid system.

Decentralized microgrid approximation model

To maintain frequency stability of $Dz\mu G$ within desired range, it is preferable to obtain an approximated FOPTD model of $Dz\mu G$ system. This is because main model consists of numerous nonlinear and highly complex equations, which leads to inefficient control design. To have an efficient FOPID control design FOPTD model is needed. The mathematical modeling of FOPTD model is depicted in (11).

$$\phi_{FOPTD}(s) = K \frac{e^{-T_d s}}{1 + sT_m} \quad (11)$$

In (11), $\phi_{FOPTD}(s)$ is the approximated first-order model of $Dz\mu G$, where K is steady-state gain, and T_m , T_d represents time constant and time delay. Using process reaction curve method^{4,46} method, FOPTD model parameters can be calculated using following equations.

$$T_d = 1.3t_1 - 0.29t_2 \quad (12)$$

$$T_m = 0.67(t_2 - t_1) \quad (13)$$

$$K = \frac{\Delta Y_\infty}{U_{\text{step}}} \quad (14)$$

where ΔY_∞ is the variation in the output signal when $t = \infty$, and the U_{step} is the amount of variation in input signal. Utilizing process reaction curve and equation (12)- (14), the $Dz\mu G$ is derived to the FOPTD model as shown in (15). Furthermore, identified FOPTD model parameters gain (K), time constant (T_m), and time delay (L) are derived and provided in tabular representation in Table 3.

Fractional order proportional-integral-derivative controller design

The motivation to use a FOPID controller over a conventional PID lies in its enhanced flexibility and superior control performance. Unlike PID, which uses integer-order integrals and derivatives, FOPID introduces

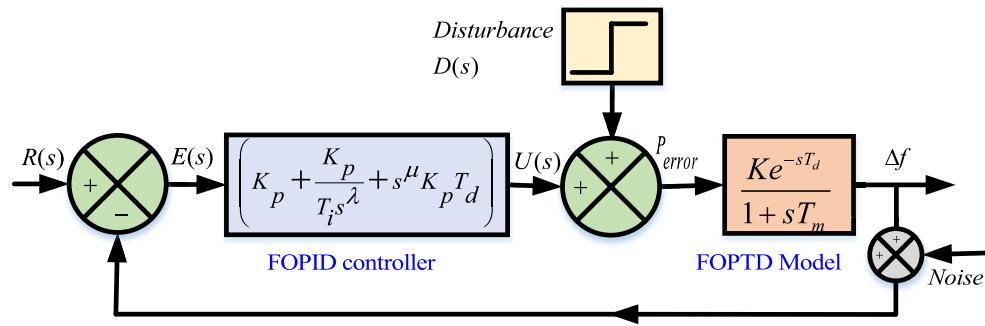


Fig. 4. Closed loop system with external load disturbances.

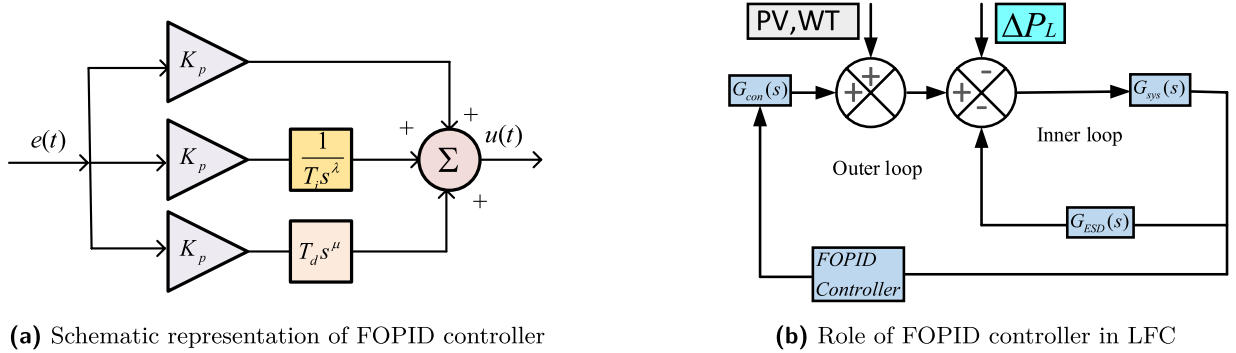


Fig. 5. Closed loop based modelling of $Dz\mu G$ components.

fractional orders (λ and μ) that provide additional tuning flexibility, enabling finer control over system dynamics. This extended degree of freedom allows FOPID to better handle complex, nonlinear, or time-delay systems often encountered in microgrids. Further, it offers improved robustness, disturbance rejection, and setpoint tracking across a wider operating range, making it particularly suitable for renewable energy integration and systems with uncertain or varying parameters.

Design method

The unity feedback control structure is shown in Fig. 4, which is considered for analyzing the dynamics of FOPTD model depicted in (15) as a plant. Fig. 4, showcased the possible inputs and disturbances which may be occurred in the system at different point.

$$\phi_{FOPTD}(s) = 9.4993 \frac{e^{-0.3951}}{1 + 2.2833s} \quad (15)$$

FOPID controller is an advanced version of the proportional-integral-derivative (PID) controller. The generalized FOPID architecture is depicted in Fig. 5a. The standard configuration of FOPID contains proportional, derivative, and integral gains, with fractional orders terms of integral (λ) and derivative (μ). The mathematical formulation of FOPID in the frequency domain is depicted in (16).

$$U(s) = K_p [1 + \frac{1}{T_i s^\lambda} + T_d s^\mu] E(s) \quad (16)$$

In (16), $U(s)$ is the FOPID output, K_p is proportional gain, T_i and T_d are integral and derivative variables and $E(s)$ is error, respectively. The implementation of FOPID controller is to regulate the active powers of controllable source such that load demand can be meet. Schematic diagram of FOPID controller implementation with controllable sources are depicted in Fig. 5b.

The dynamics of the process are described by normalized dead time τ which is defined as $\tau = \frac{T_d}{T_m}$, where T_d is time delay and T_m is time constant of FOPTD model. The normalized dead time gives a measure of difficulty in controlling the process. In general, the values of the normalized dead time in the range of $0.01 \leq \tau \leq 4$ is considered⁴⁹. The value of τ for presented $Dz\mu G$ model is 0.1730. To design efficient controller, fine tuning of FOPID controller is important. To derive suitable gains, the FOPID controller utilizes the ISE and ITSE error indices as performance indices, which are depicted in (17) and (18).

$$ISE = \int_0^\infty |e(t)|^2 dt \quad (17)$$

$$ITSE = \int_0^\infty t|e(t)|^2 dt \quad (18)$$

Minimizing ISE results in reduced overshoot and minimum settling time simultaneously in LDR or SPT control responses. A controller is said to have robustness when it is not sensitive to parameter variations or uncertainties. To improve the robustness of the FOPIID controller, the controller has been designed to minimize the ISE and maximize sensitivity as a constraint. The maximum sensitivity (M_s) is represented (19) as

$$M_s = \max_{w \in [0, \infty]} \left| \frac{1}{1 + G(s)C(s)H(s)} \right|_{s=jw} \quad (19)$$

Where $G(jw)$ controller transfer function and $C(jw)$ plant transfer function. M_s represents the inverse of the shortest distance from the Nyquist curve.

Tuning of optimal controller

To obtain FOPIID parameters, the tuning rules of a controller for the control of frequency deviation, Bayat method is preferred and implemented⁵⁰. The set point control and disturbance rejection tasks have been performed separately to minimize the ISE with two values of maximum sensitivity such as $M_s = 1.4$ and $M_s = 2.0$. For $M_s = 1.4$, a system has more robustness, and for $M_s = 2.0$, the aggressiveness is more important. A detailed description of bayat tuning methodology and its implementation in FOPIID control design is discussed in Fig. 6.

Bayat method: ISE based tuning method

The mathematical formulation of FOPIID gains as per Bayat et al^{49,51} are expressed in (20), (21), (22), and (23), respectively.

$$K_p = \frac{1}{k} * \frac{(0.3663\tau + 0.8856)}{\tau + 0.00092} \quad (20)$$

$$T_i = T * (0.3827\tau + 0.9354) \quad (21)$$

$$T_d = T * (0.5036\tau^{0.7152} - 0.07974) \quad (22)$$

$$\mu = -0.03625\tau + 1.095 \quad (23)$$

Bayat method: ISE-based tuning method for load disturbance

The mathematical formulation of FOPIID gains as per Bayat et al^{49,51} are expressed in (24), (25), (26), and (27), respectively.

$$K_p = \frac{1}{k} * \frac{(0.2709\tau + 1.566)}{\tau + 0.0364} \quad (24)$$

$$T_i = T * (1.252\tau^{0.5555} - 0.05696) \quad (25)$$

$$T_d = T * (0.3425\tau + 0.02753) \quad (26)$$

$$\mu = -1.368\tau^{0.04705} + 2.503 \quad (27)$$

Bayat method: ITSE-based tuning method

The mathematical formulation of FOPIID gains as per Bayat et al^{49,51} are expressed in (28), (29), (30), and (31), respectively.

$$K_p = \frac{1}{k} * \frac{(0.3517\tau + 0.8494)}{\tau + 0.00066} \quad (28)$$

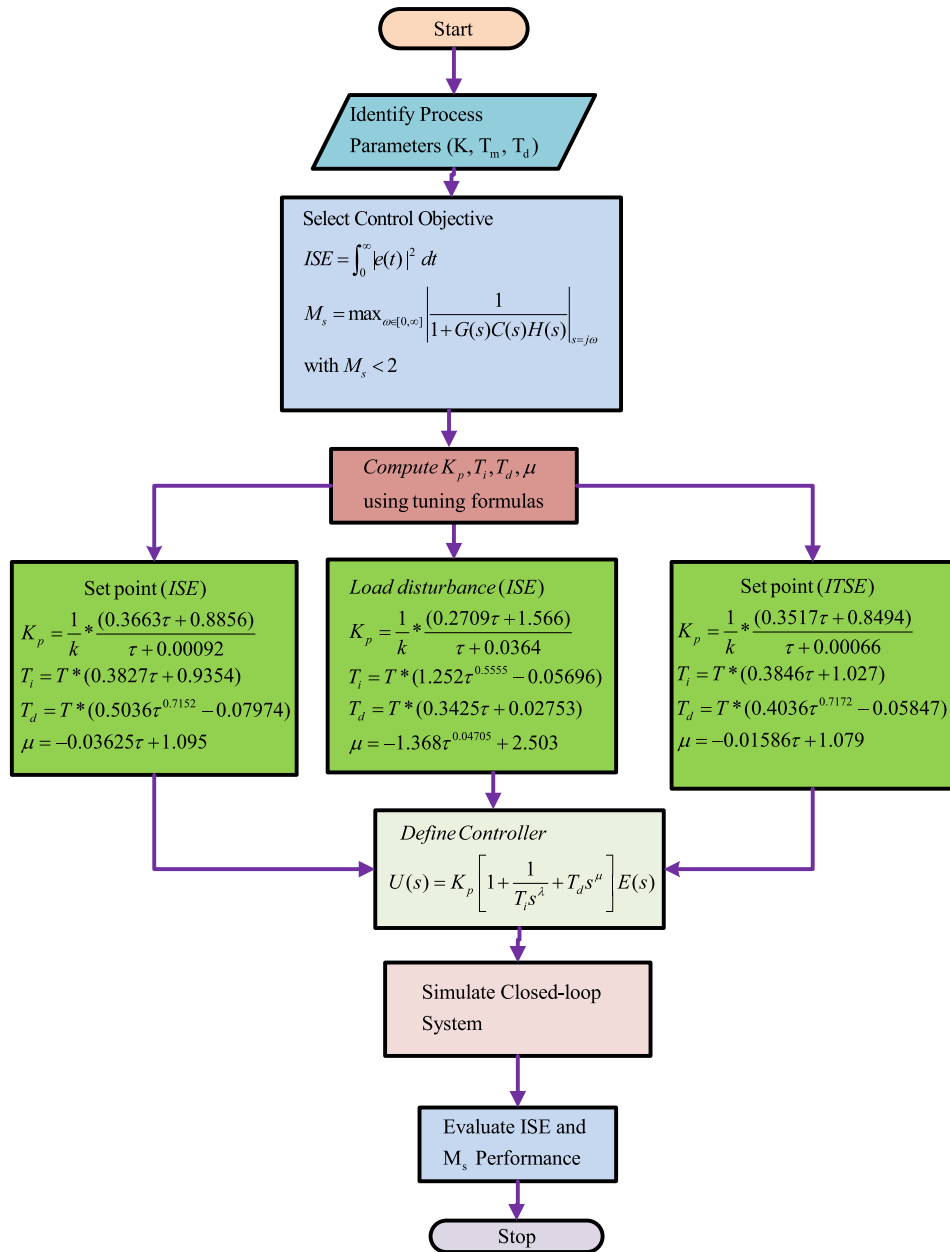
$$T_i = T * (0.3846\tau + 1.027) \quad (29)$$

$$T_d = T * (0.4036\tau^{0.7172} - 0.05847) \quad (30)$$

$$\mu = -0.01586\tau + 1.079 \quad (31)$$

Variable τ can be defined as

$$\tau = \frac{L}{T} \quad \tau \in [0.1, 4] \quad (32)$$

**Fig. 6.** Flowchart of FOPID controller.**Oustaloup approximation method**

To analyze and implement fractional order of integral (λ) and derivative terms (μ), approximation methods are utilized. These methods approximate fractional-order terms into integer-order equivalents within fixed bandwidth. Numerous approximation methods are available in literature⁵². Oustaloup approximation is a widely accepted method for approximation purposes⁵³. The Oustaloup approximation method utilizes the recursive scattering of poles and zeroes to derive equivalent integer order from fractional order. The mathematical representation of fractional term (s^a) using the Oustaloup approximation method is given in (33).

$$s^a \approx K \prod_{m=1}^N \frac{1 + (s/w_{z,n})}{1 + (s/w_{p,n})}, a > 0 \quad (33)$$

where, K is static gain, and $w_{z,n}$, $w_{p,n}$ denoted frequencies corresponding to zeros and poles, respectively. The Zeros $w_{z,n}$ and poles $w_{p,n}$ are given as in Eqs. (34)

$$w_{z,n} = w_l \left(\frac{w_h}{w_l} \right)^{\frac{m+N+(1-r)/2}{2n+1}}$$

$$w_{p,n} = w_l \left(\frac{w_h}{w_l} \right)^{\frac{m+N+(1-r)/2}{2N+1}} \quad (34)$$

In (34), w_l and w_h represent minimum and maximum limits of frequency of approximation in the range $\omega \in [0.001w_c, 1000w_c]$ such that $w_l w_h = 1$. In simulation, the designed FOPID controller is approximated using Oustaloup method. The frequency range considered for approximation is 0.001–1000 rad/sec with approximation order of 5.

Results and discussion

Frequency response without controller

Before implementing a controller, it is essential to analyze the frequency response of microgrid model. The frequency response of $G_{Dz\mu G}(s)$ model is illustrated in Fig. 7a. This response can be evaluated using standard transient performance indicators such as rise time (0.1698 s), settling time (8.0089 s), peak time (0.6222 s), peak value (0.4673 pu), undershoot (258.5687), and overshoot (80.9992). The system exhibits significant overshoot and undershoot, along with underdamped oscillations, with offset error of 0.1803 pu. Such deviations are undesirable, as the desired frequency deviation is zero. In this contribution, Δf is the control parameter which is to be minimized through FOPID controller.

To further assess the system performance, various error indices have been computed. The integral absolute error (IAE) is 9.182, the integral time absolute error (ITAE) is 225.9, the integral squared error (ISE) is 1.756, and the integral time squared error (ITSE) is 40.9. These values highlight the poor dynamic performance of the system. However, these deficiencies evident in both transient response and error indices can be effectively mitigated by integrating a FOPID controller into the $G_{Dz\mu G}$ model.

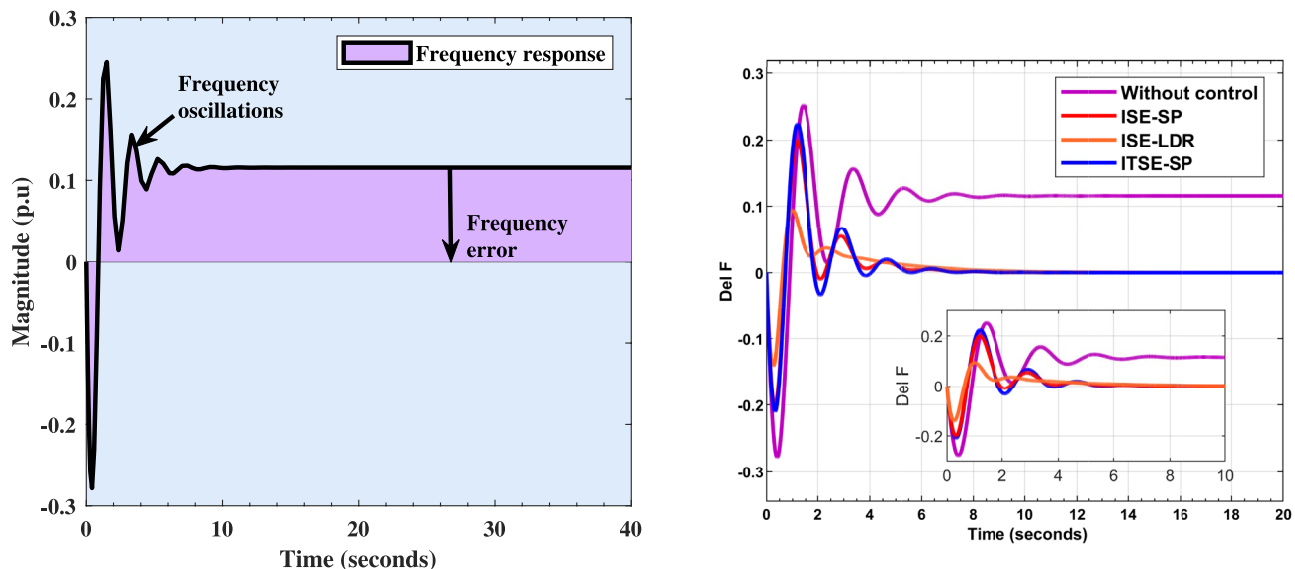
Frequency response with FOPID controller

To suppress the deviations and eliminate the offset error of the frequency response, various variants of the FOPID controller are designed. These controllers are identified as FOPID-Bayat_{SP1.4}, FOPID-Bayat_{SP2.0}, and FOPID-Bayat_{LD1.4}. These controller designs are formulated using the tuning methodology i.e. Bayat method for SPT and LDR scenarios with maximum sensitivity ($M_s = 1.4$ and $M_s = 2.0$). The gains of designed FOPID controllers are obtained using Bayat method for both modes, which are given in Table 4. The mathematical formulation of all designed FOPID controllers are presented in (35)–(37).

$$C_{\text{FOPID-Bayat}_{\text{SP1.4}}}(s) = \frac{1.35950332 s + 1.5596 + 0.137581735984 s^{2.0850}}{0.8717 s}$$

$$C_{\text{FOPID-Bayat}_{\text{SP2.0}}}(s) = \frac{1.39339309 s + 2.9959 + 0.142404773798 s^{2.2154}}{0.4651 s}$$

$$C_{\text{FOPID-Bayat}_{\text{LD1.4}}}(s) = \frac{1.41058096 s + 1.4867 + 0.120322555888 s^{2.076}}{0.9488 s}$$



(a) Frequency response of decentralized microgrid

(b) Dynamic frequency response of microgrid under different control designs

Fig. 7. Frequency response of decentralized microgrid with and without FOPID controller.

Gains	FOPID-Bayat _{SP1.4}	FOPID-Bayat _{SP2.0}	FOPID-Bayat _{LD1.4}
K_p	1.5596	2.9959	1.4967
T_i	0.8717	0.4651	0.9488
T_d	0.1012	0.1022	0.0853
λ	1	1	1
μ	1.0850	1.2154	1.0767

Table 4. FOPID controller gains for frequency regulation of $G_{Dz\mu}G(s)$ Model.

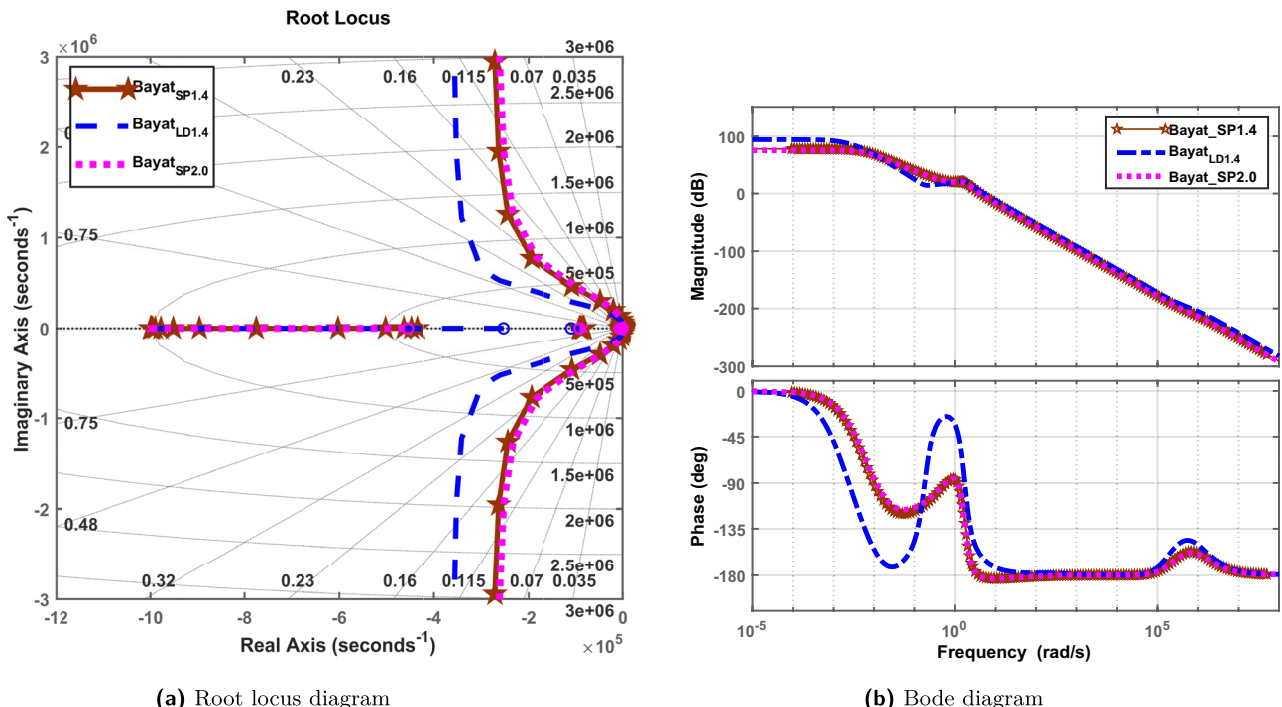


Fig. 8. Root locus and bode diagram.

$$C_{FOPID-Bayat_{SP1.4}} = 1.5596 \left[1 + \frac{1}{0.8717s^1} + 0.1012s^{1.0850} \right] \quad (35)$$

$$C_{FOPID-Bayat_{SP2.0}} = 2.9959 \left[1 + \frac{1}{0.4651s^1} + 0.1022s^{1.2154} \right] \quad (36)$$

$$C_{FOPID-Bayat_{LD1.4}} = 1.4967 \left[1 + \frac{1}{0.9488s^1} + 0.0853s^{1.076} \right] \quad (37)$$

In (35)-(37), $C_{FOPID-Bayat_{SP1.4}}$, $C_{FOPID-Bayat_{SP2.0}}$, $C_{FOPID-Bayat_{LD1.4}}$, are FOPID controller transfer functions for SPT and LDR modes, respectively. All variants of Bayat-tuned FOPID controllers ($C_{FOPID-Bayat_{SP1.4}}$, $C_{FOPID-Bayat_{SP2.0}}$, and $C_{FOPID-Bayat_{LD1.4}}$), are implemented to eliminate deviations occurring in the frequency response of the model. The dynamic frequency response of the microgrid with the controllers discussed is discussed in Fig. 7b. From figure it is clear that, all discussed controllers mitigate the offset error and maintain a frequency stability with improved transient response. 8.

Stability analysis

To ensure stability of the microgrid and its control designs, root locus plot and bode plots are provided in Fig. 8a and b. For this study, the frequency domain stability analysis is carried out through bode plots to validate the stability performance of the proposed control scheme. Figure 8 provides a comparative analysis of the closed-loop dynamics for three Bayat-tuned FOPID controllers—Bayat_{SP1.4}, Bayat_{LD1.4}, and Bayat_{SP2.0}—through root locus and Bode plots. Fig. 8a presents the root locus diagram, illustrating the pole migration paths as system gain varies. It is evident that all three controllers shift the dominant poles toward the left half of the s-plane, indicating enhanced system stability. Among them, Bayat_{SP1.4} and Bayat_{LD1.4} exhibit superior damping characteristics with poles closer to the real axis, resulting in a faster and more stable response. Bayat_{SP2.0} shows

comparatively less damping, with some poles near the imaginary axis, suggesting higher oscillatory behavior under dynamic conditions. Fig. 8b shows the Bode diagram, providing insight into the frequency response characteristics of the controllers. In the magnitude plot, all designs maintain adequate gain margins across the frequency range, ensuring robust performance. The phase response reveals that Bayat_{SP1.4} and Bayat_{LD1.4} maintain better phase stability over the mid-frequency band compared to Bayat_{SP2.0}, which exhibits a pronounced phase dip. These observations collectively affirm that Bayat_{SP1.4} and Bayat_{LD1.4} offer better control authority, phase margin, and robustness to dynamic variations in the microgrid system. Eigenvalues of FOPID-Bayat_{SP1.4}, FOPID-Bayat_{SP2.0}, and FOPID-Bayat_{LD1.4} controllers are $-1.0000 + 0.0000i$, $-0.0811 + 0.0000i$, $-0.0066 + 0.0000i$, $-0.0005 + 0.0000i$, $-0.0001 + 0.0000i$, $-0.0000 + 0.0000i$.

In this contribution, three versions of FOPID controller, i.e., $C_{FOPID-Bayat_{SP1.4}}$, $C_{FOPID-Bayat_{SP2.0}}$, and $C_{FOPID-Bayat_{LD1.4}}$ are discussed for frequency control of microgrid. A comparative analysis is performed among the discussed FOPID controller, and their performances are analyzed in terms of convergence speed, frequency stability, error indices, and control effort for cases which are mentioned here as

- Case 1. Random load disturbances.
- Case 2. Solar power variations.
- Case 3. Wind power variations.
- Case 4. Parameter variation.
- Case 5. Multiple disturbances test case.
- Case 6. Real-time validation.

FOPID controller design and validation for random load disturbance

In this study, a scenario involving random load variations is analyzed to evaluate the performance of the proposed control strategy. Specifically, the system is subjected to a composite loading profile that includes a base load of 0.2 per unit (p.u), a domestic load component of 0.6 p.u, and an industrial load of 0.8 p.u. These variations aim to simulate realistic demand conditions that a $Dz\mu G$ model may encounter during its operation. In this contribution, considered penetration levels of wind, solar, Biogas, and Biodiesel are 50%, 50%, 30%, and 25%, respectively. The composite profile of these load changes is illustrated in Fig. 9a, which shows the sequence and magnitude of the applied load steps over time.

The frequency response due to FOPID-Bayat_{SP1.4}, FOPID-Bayat_{SP2.0}, and FOPID-Bayat_{LD1.4} for multiple load variations is presented in Fig. 9b. As observed from the figure, the proposed FOPID controller eliminated offset errors with improved transient performance. Transient response indicators of frequency response corresponding to this case are mentioned in Table 5. This includes reduced overshoot, faster settling time, and better frequency regulation during abrupt load transitions.

Furthermore, the controller effort, which reflects the signal required to maintain system stability and performance for FOPID-Bayat_{SP1.4}, FOPID-Bayat_{SP2.0}, and FOPID-Bayat_{LD1.4} for multiple load variations, is shown in Fig. 9c. It is evident from this figure that the Bayat-tuned FOPID controller not only enhances the dynamic response but also operates more efficiently by minimizing excessive control actions. This balance between performance and control effort underscores the effectiveness of the proposed controller.

FOPID controller design and validation for solar power variations

The variation in solar power generation over the course of a typical day is illustrated in Fig. 10a. In this contribution, the penetration levels of solar are considered to be 50%. This profile represents the natural fluctuation in solar irradiance due to factors such as the sun's position and environmental conditions. These variations introduce disturbances to the microgrid. To assess the FOPID-Bayat_{SP1.4}, FOPID-Bayat_{SP2.0}, and FOPID-Bayat_{LD1.4} controller's capability to maintain frequency stability under solar variations, frequency response is presented in Fig. 10b. The results indicate that the Bayat-tuned FOPID controllers effectively mitigate the adverse effects of solar intermittency. A quantitative assessment of the frequency response for solar power variations is summarized in Table 5. This table concludes that the FOPID-Bayat_{SP1.4}, FOPID-Bayat_{SP2.0}, and FOPID-Bayat_{LD1.4} control designs provide better oscillation damping, faster stabilization, and reduced frequency deviations.

Additionally, the control efforts required by the various controllers to sustain frequency stability during the solar power variations are shown in Fig. 10c. From this figure, it is clear that the proposed FOPID controller not only achieves enhanced dynamic performance but requires relatively lower control effort, highlighting its efficiency and robustness.

FOPID controller design and validation for wind power variations

The variation in wind power generation, which inherently results from the stochastic and intermittent nature of wind speed, is illustrated in Fig. 12a. In this contribution, considered penetration levels of wind are 50%. These fluctuations are a common challenge in microgrid operation, as they introduce significant disturbances to system frequency and demand effective control mechanisms to ensure stable operation. The frequency response of $Dz\mu G$ model under the influence of multiple load variations is shown in Fig. 12b. FOPID-Bayat_{SP1.4}, FOPID-Bayat_{SP2.0}, and FOPID-Bayat_{LD1.4} controllers provide improved frequency regulation, reduced overshoot, and faster settling during this case. The control efforts of FOPID-Bayat_{SP1.4}, FOPID-Bayat_{SP2.0}, and FOPID-Bayat_{LD1.4} controllers to maintain frequency stability during wind variations are presented in Fig. 12c. As seen from the figure, the FOPID-Bayat_{SP1.4}, FOPID-Bayat_{SP2.0}, and FOPID-Bayat_{LD1.4} controllers maintain system stability with comparatively lower

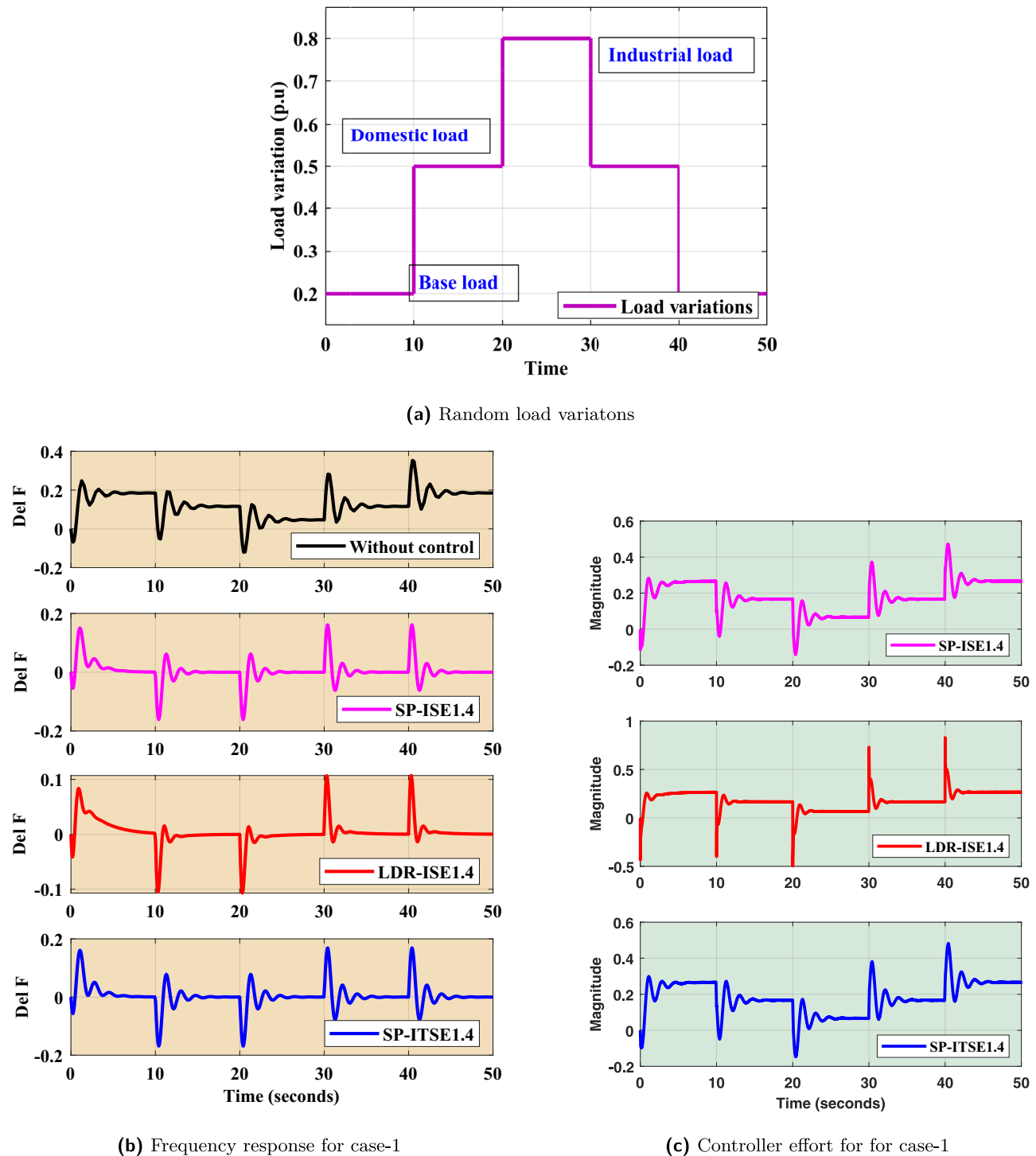


Fig. 9. Case 1: Random load disturbances.

control magnitude, emphasizing its efficiency and robustness in the presence of high variability. Further, efficacy of FOPID-*Bayat*_{SP1.4}, FOPID-*Bayat*_{SP2.0}, and FOPID-*Bayat*_{LDR1.4} controllers are analysed through error indices, which are mentioned in Table 6. Additionally, a statistical analysis of the frequency response during the wind power variation scenario is included in Table 5 to prove the efficacy of control designs.

Multiple disturbances test case

The impact of multiple power variations from wind turbine (WT), photovoltaic (PV), and load (P_L) sources—is illustrated in Fig. 13. Figure 13a displays the normalized power variation profiles of P_{WT} , P_{PV} , and P_L over time, reflecting a typical scenario with high variability and intermittent renewable inputs. This dynamic

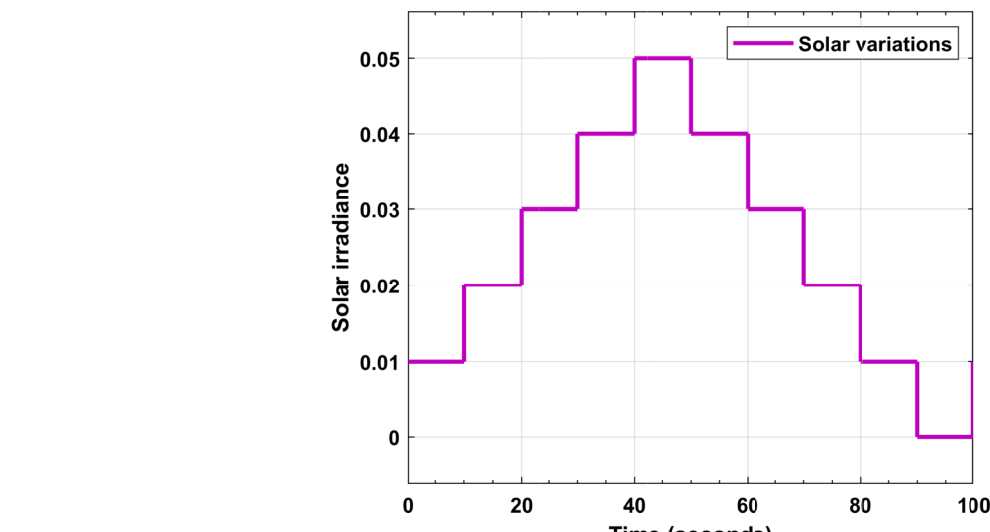
Controller's		FOPID-Bayat _{SP1.4}	FOPID-Bayat _{SP2.0}	FOPID-Bayat _{LDR1.4}
Scenario's	Specifications			
Case 1	T_r	4.99e - 5	6.31e - 4	1.79e - 4
	T_p	30.3985	40.3116	30.4056
	$\%O_s$	5.136e5	4.9531e4	1.5077e5
	T_s	49.8586	49.9534	49.9330
	Controllability	Yes	Yes	Yes
	control effort	0.285	0.25	0.295
Case 2	T_r	4.0219e-5	2.2123e-4	1.2179e-4
	T_p	0.8353	.7316	0.8327
	$\%O_s$	1.14e7	5.2163e4	3.899e6
	T_s	49.8498	49.9552	49.9315
	Controllability	Yes	Yes	Yes
	control effort	0.32	0.33	0.353
Case 3	T_r	6.4248e-5	0.0087	2.3681e-4
	T_p	0.8186	0.7161	0.8153
	$\%O_s$	5.3477e5	6.1249e4	1.5181e5
	T_s	49.8615	49.9535	49.9331
	Controllability	Yes	Yes	Yes
	control effort	0.33	0.32	0.34
Case 4	T_r	6.4248e-5	0.0308	3.3681e-4
	T_p	0.7186	0.6161	0.5153
	$\%O_s$	5.4547e5	6.1794e4	1.581e5
	T_s	49.615	49.535	49.331
	Controllability	Yes	Yes	Yes
	control effort	0.17	0.12	0.15

Table 5. Statistical analysis of the proposed controllers.

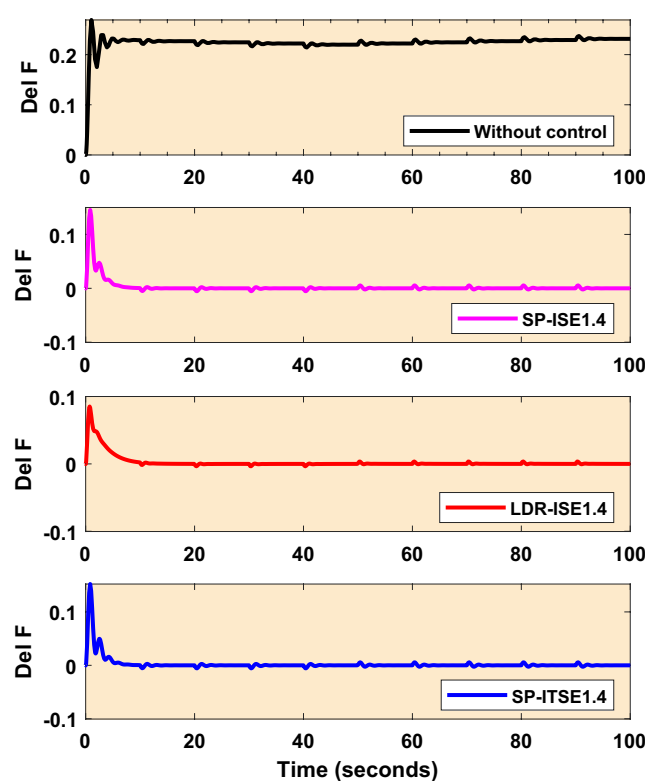
environment poses a significant challenge to microgrid frequency stability and requires robust control strategies to maintain operational resilience. Figure 13b presents the frequency response of the $Dz\mu G$ system for Case-4 under the influence of these variations. In the absence of control, the system exhibits pronounced frequency deviations, confirming the destabilizing effect of renewable intermittency and load fluctuations. In contrast, the implementation of fractional-order PID (FOPID) controllers—namely SP-ISE1.4, LDR-ISE1.4, and SP-ITSE1.4—significantly improves frequency regulation. These controllers effectively reduce frequency deviation, enhance damping, and achieve quicker settling times. The associated control efforts are shown in Fig. 13c. All three controllers demonstrate adequate actuation with reasonable control signal magnitudes, ensuring frequency stabilization without introducing excessive control action. Among them, SP-ISE1.4 and SP-ITSE1.4 exhibit smoother transitions, suggesting better performance under the fluctuating power conditions of Case-4. This validates the proposed FOPID control designs as robust and efficient solutions for maintaining microgrid frequency stability in the presence of diverse and time-varying disturbances.

Frequency analysis under stochastic load

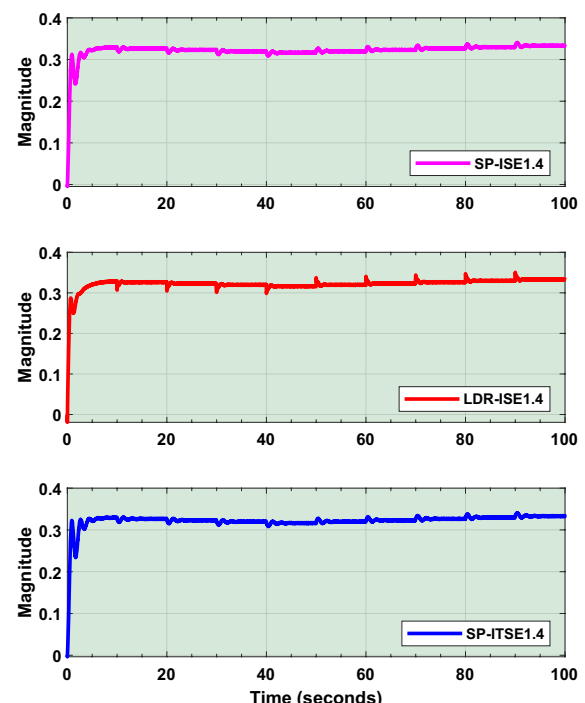
Figure 14 illustrates the performance of the proposed control strategies under a stochastic load disturbance scenario. Figure 14a depicts the randomly varying power input profile used to emulate real-world uncertainties and rapid fluctuations in load demand. Such stochastic variations pose significant challenges to microgrid frequency stability and demand resilient control designs. The corresponding frequency responses for Case-4 are shown in Fig. 14b. In the absence of control, the system experiences large and sustained frequency deviations, reflecting poor disturbance rejection capability. In contrast, the application of FOPID controllers—SP-ISE1.4, LDR-ISE1.4, and SP-ITSE1.4—leads to substantial improvements in frequency regulation. These controllers successfully mitigate the impact of stochastic disturbances, as seen by reduced oscillation magnitudes and enhanced damping behavior. Figure 14c presents the associated control efforts for each controller. Despite the erratic nature of the load input, all three controllers maintain stable and bounded control signals. Notably, SP-ITSE1.4 demonstrates the most efficient control effort with reduced actuation magnitudes, indicating better control economy and robustness. The overall performance confirms the effectiveness of the proposed Bayat-tuned FOPID controllers in preserving microgrid frequency stability under highly uncertain and non-deterministic load conditions.



(a) Solar power variations



(b) Frequency response for case-2



(c) Controller efforts for case-2

Fig. 10. Case 2. Solar power variations.

Sensitivity analysis

In this study, sensitivity analysis is performed considering parametric variations in time constant of T_{bdeg} , T_{bgtg} , as these are the more sensitive component of the presented model. A variation of ± 50 in the range of 25% i.e., $(-50, -25, +25, +50)$ is considered for the analysts purpose. Moreover, same variation is applied to damping (D) and inertia constant (M) of model to study behavioral changes of $Dz\mu G$ model due to these variations. Statistical analysis based on the parametric variation is provided in Table 7. Moreover, impact of these parameters on Δf is also depicted in Table 7. Additionally, the impact of parametric analysis are understood by transient response indicators i.e., T_s , T_p , T_r , and various error indices such as IAE, ITAE, ISE, ITSE.

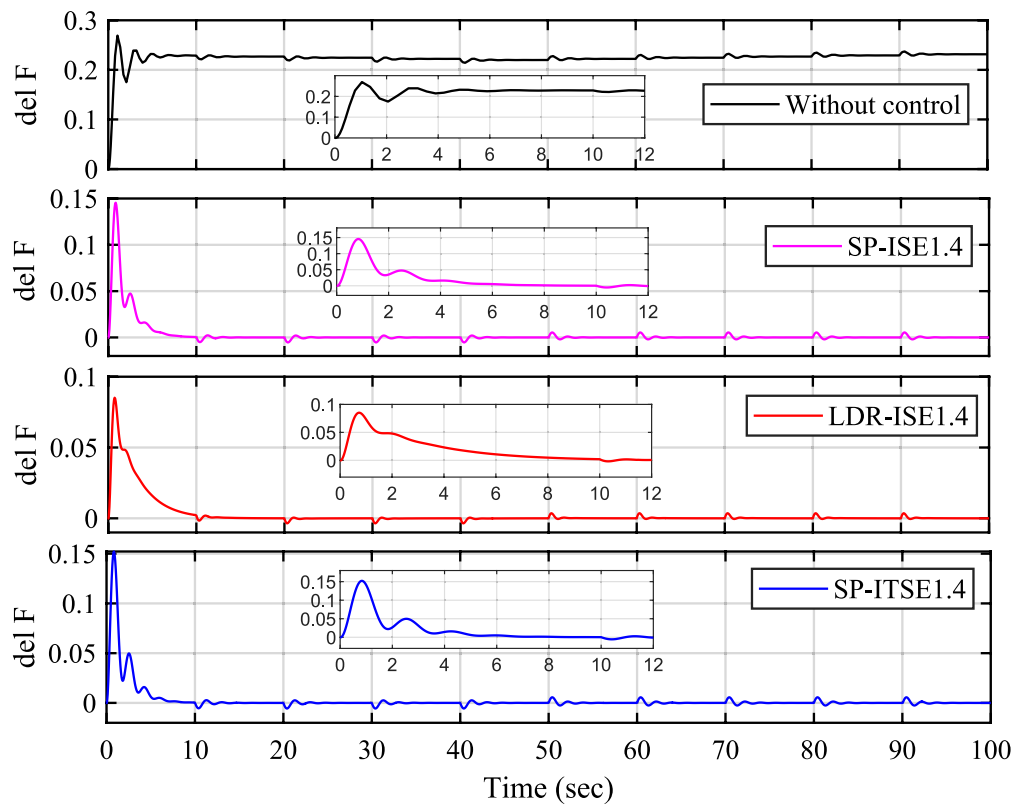


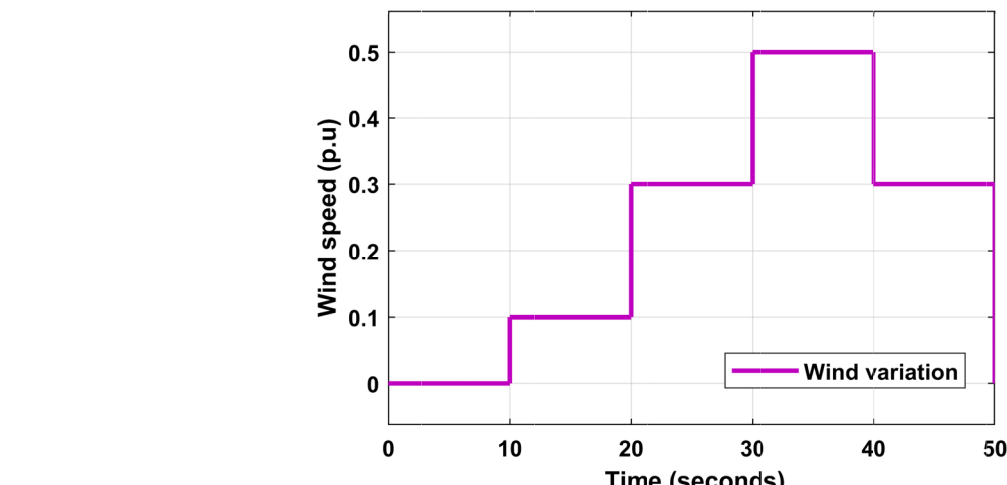
Fig. 11. Frequency response for case-2.

Real-time validation

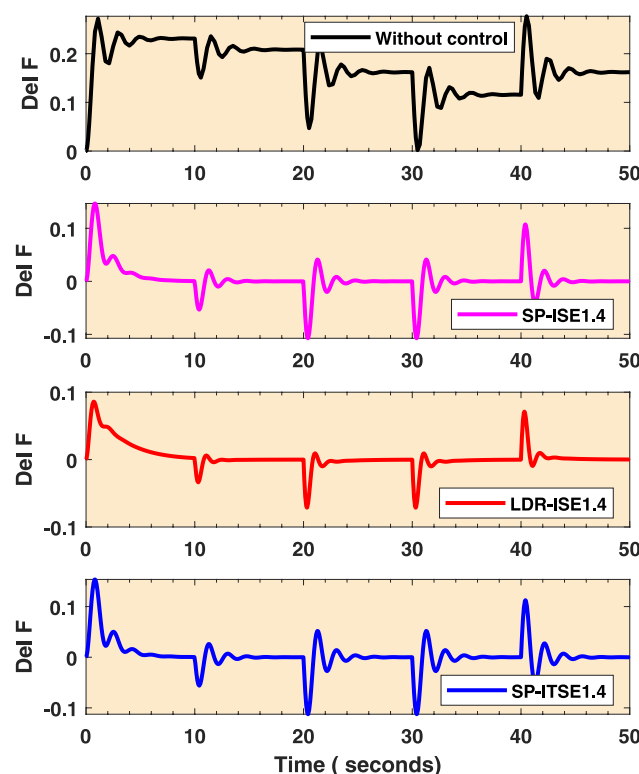
To validate the real-time performance of the discussed version of FOPID controller, OP5600 Opal-RT real-time simulator is used, which is depicted in Fig. 15a. It is a high-performance platform equipped with a 12-core processor, ideal for complex real-time simulations. The system includes OP5142 analog output cards, which ensure accurate signal transfer to external devices. For output visualization, the simulator is connected to a Yokogawa DL950 oscilloscope via Mini-BNC to BNC cables, enabling direct monitoring and capture of signals from the simulator's output port. Furthermore, a real-time validation procedure using OPAL-RT is provided in algorithm 1. Furthermore, the experimental setup details are as follows,

- Sampling frequency: 20 kHz
- Signal scaling for analog/digital interfaces
- Use of RT-LAB's scaling blocks and anti-aliasing filters
- Latency compensation: No explicit compensation used due to low-latency (<1 ms) setup; this is now noted and justified

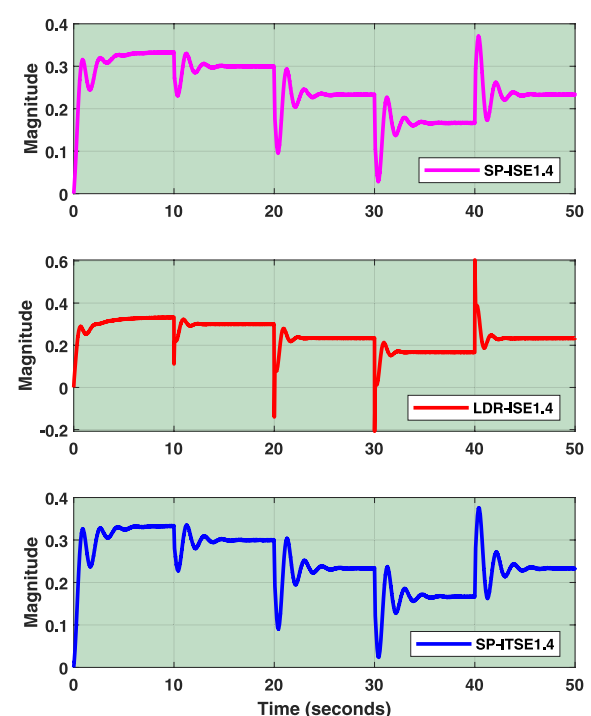
Various version of FOPID controllers are tested on OPAL-RT simulator to test the feasibility of control design and their effectiveness in maintaining frequency responses of $Dz\mu G$ model. The frequency response of $Dz\mu G$ model using various FOPID controllers via MATLAB without considering delay is provided in Fig. 15b. The OPAL-RT based frequency response of various FOPID controllers is depicted in Fig. 15c. Based on Fig. 15b and c, it is observed that frequency responses are equivalent, which justify the FOPID control designs.



(a) Wind power variations



(b) Frequency response for case-3

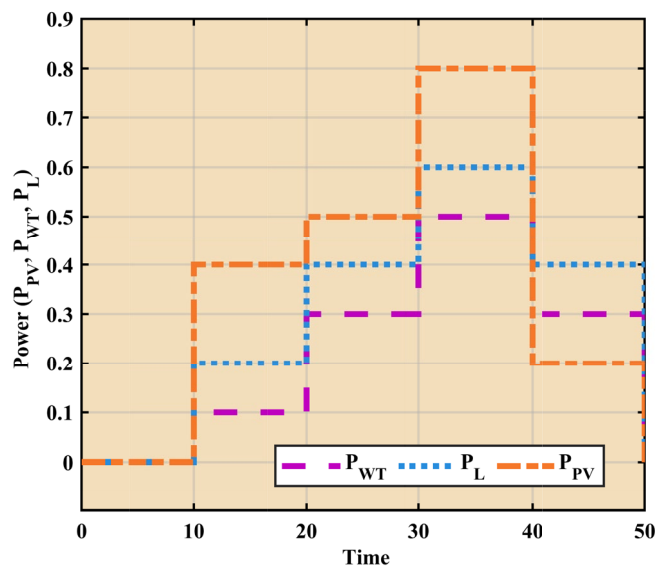


(c) Controller effort for case-3

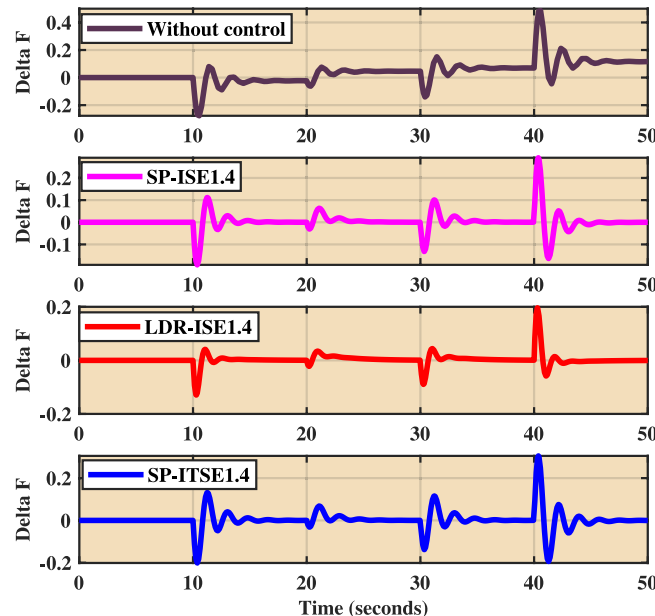
Fig. 12. Case 3. Wind power variations.

Error Index	FOPID-Bayat _{SP1.4}	FOPID-Bayat _{SP2.0}	FOPID-Bayat _{LD1.4}
IAE	9.336	8.737	15.180
ITAE	223.5	223.0	280.0
ITSE	41.86	40.39	98.20
ISE	2.318	1.706	8.029

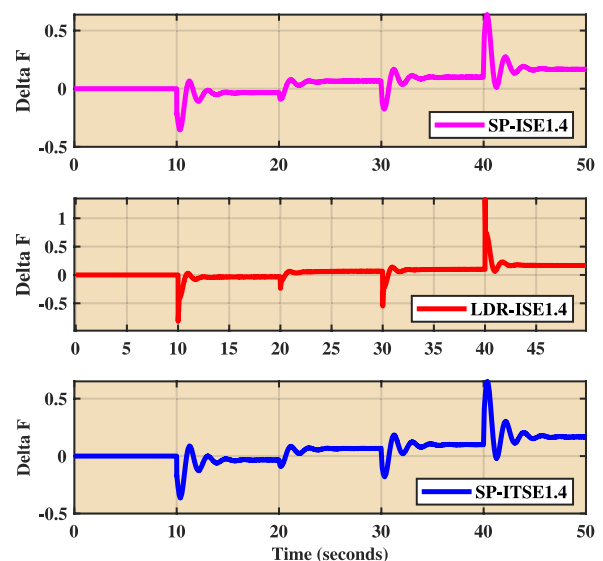
Table 6. Comparison of different error indices for various FOPID tuning rules.



(a) Multiple power variations

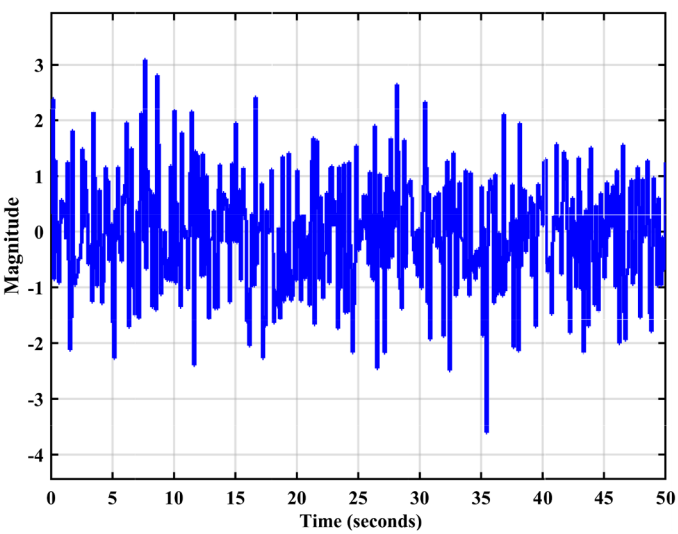


(b) Frequency response for case-4

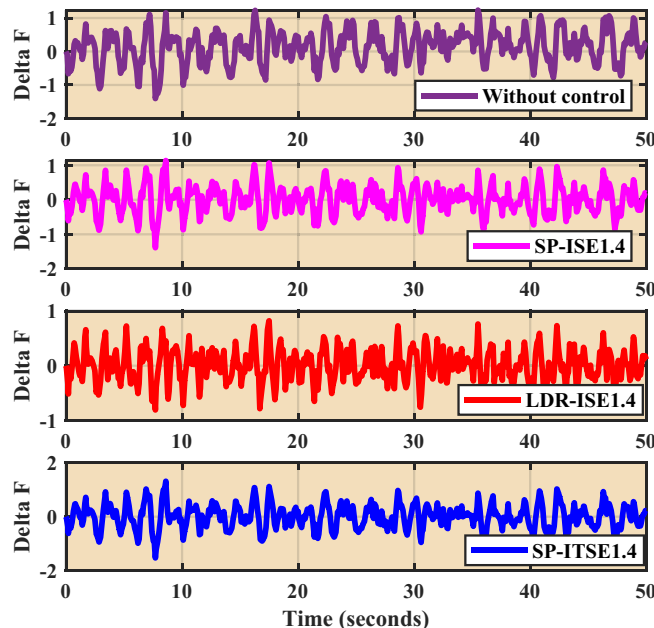


(c) Controller effort for case-4

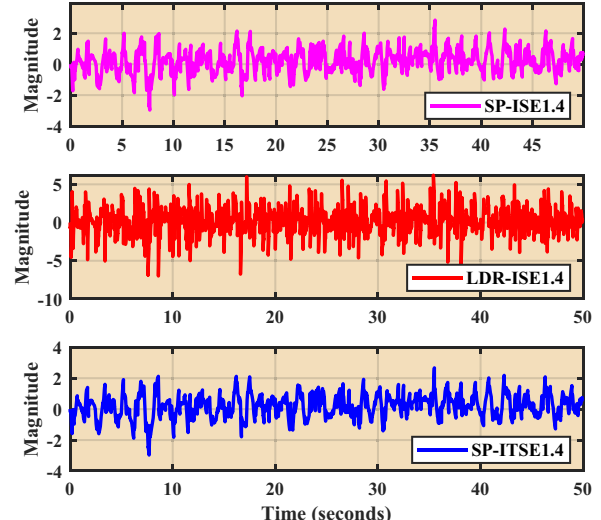
Fig. 13. Case 4. Multi-disturbance test case.



(a) Uncertainty



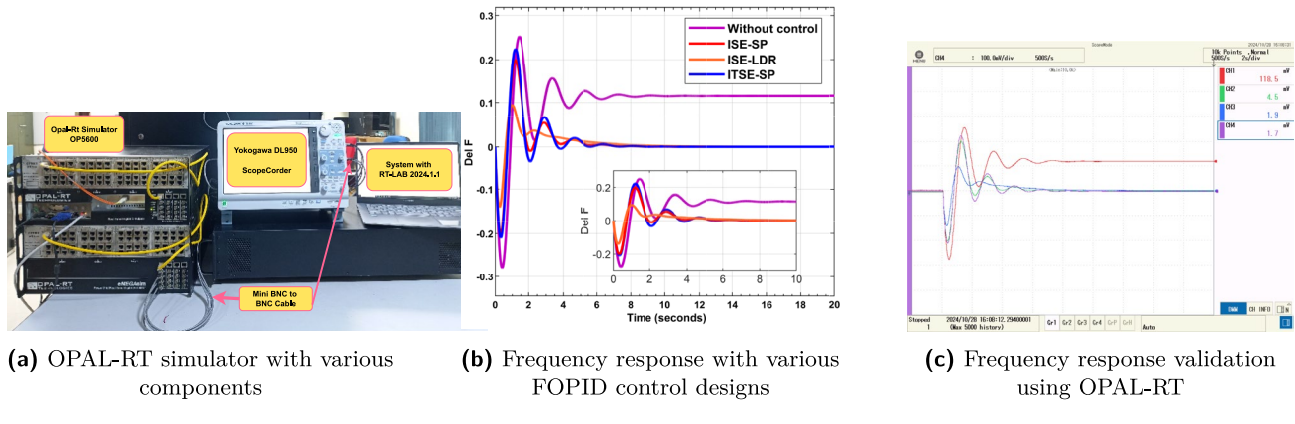
(b) Frequency response for case-4



(c) Controller effort for case-4

Fig. 14. Frequency analysis under stochastic load.

	(%)	$Ts(s)$	$Tp(s)$	$Tr(s)$	IAE	ITAE	ISE	ITSE	Δf
T_{bdeg}	-50	9.9687	.8272	6.9789	0.02106	0.2419	0.01597	.4898	.00042
	-25	9.9687	0.8213	0.0099	0.02091	0.2419	0.1698	0.4787	.0004203
	+25	9.9674	.8503	0.0110	0.02285	.2419	0.02016	.4566	.0004848
	+50	9.9758	.8663	.0115	.02418	.2418	.02209	.445	.0005121
T_{bgtg}	-50	9.9665	.7850	.0137	.01994	.2415	.01508	.5228	.0006433
	-25	9.9681	.8140	.0122	.0206	.2416	.01684	.4946	.0005908
	+25	9.9786	.8505	.0060	.02253	.2423	.01978	.4429	.0002269
	+50	9.9930	.8630	9.7485e4	.02357	.2429	.02097	.4208	-2.928e-5
D	-50	9.9739	0.8353	0.0099	.02159	.2419	.01853	.4669	.0004178
	-25	9.9734	0.8349	0.0099	.02155	.2419	.01847	.4673	.0004182
	+25	9.9726	0.8354	0.0099	.02148	.2419	.01835	.4681	.0004191
	+50	9.9723	0.8353	0.0090	.02145	.2419	.01832	.4686	.0004195
M	-50	9.9686	0.6133	0.0058	.01907	.2419	.01677	.4675	.0004262
	-25	9.9693	0.7331	0.0080	.02021	.2419	.01762	.4676	.0004221
	+25	9.9591	0.9237	0.0106	.02299	.2419	.01916	.4678	.0003694
	+50	9.9793	1.0043	0.0154	.02461	.2419	.0189	.4680	.0005122

Table 7. Parametric variations.**Fig. 15.** Real time validation.

```

1: procedure REALTIMEVALIDATION PROCEDURE
2:   Load the Simulink model: DzμG_with_FOPID
3:   Verify model compatibility with RT-LAB requirements
4:   Partition the model into Console and Target subsystems
5:   Launch RT-LAB software
6:   Import the Simulink model into RT-LAB
7:   Assign the Target subsystem to OP5600 hardware
8:   Configure simulation parameters (solver type, step size, external mode)
9:   Generate C code using Simulink Coder
10:  Compile and deploy the real-time executable to OP5600
11:  Connect I/O ports and ScopeCorder (DL950)
12:  Start the simulation via RT-LAB
13:  while simulation is running do
14:    Acquire real-time data from OP5600
15:    Display and log data using the ScopeCorder
16:    Monitor key variables: frequency (f), control signal (u)
17:  end while
18:  Stop the simulation
19:  Extract recorded data from the DL950
20:  Compare real-time results with offline simulation outcomes
21:  Evaluate FOPID controller performance metrics
22: end procedure

```

Algorithm 1. Real-Time Validation Procedure Using OPAL-RT

Conclusion

This article investigates the Bayat method for frequency stability of a decentralized microgrid model by designing FOPID controllers. To implement FOPID controller, a linear transfer function of $Dz\mu G$ model is obtained. To approximate the transfer function of $Dz\mu G$ model, it is linearized and approximated as FOPTD model. FOPID control design is derived for set point tracking and load disturbance rejection modes. A comparative assessment of variants of FOPID controllers is performed to ascertain the suitable control design to maintain frequency stability of decentralized microgrids. Among the utilized tuning methods such as FOPID-*Bayat_{SP1.4}*, FOPID-*Bayat_{SP2.0}*, and FOPID-*Bayat_{LD1.4}*, FOPID-*Bayat_{SP2.0}* emerges as a suitable and efficient control design for frequency error mitigation of the $Dz\mu G$ model. The results showcased in this study highlight the efficacy of the FOPID-*Bayat_{SP2.0}* method concerning transient response, control signal magnitude, and frequency deviation plots. The statistical and error index analyses validate the superiority of the proposed controllers across all scenarios. All FOPID-*Bayat* configurations maintained controllability, with rise times as low as 4.02×10^{-5} s and settling times remaining stable around 49.8 s. The control effort was minimized to 0.12, indicating improved efficiency. In addition, FOPID-*Bayat_{SP2.0}* demonstrated the best error performance, with minimum IAE (8.737), ITAE (223.0), ITSE (40.39), and ISE (1.706). These findings establish FOPID-*Bayat_{SP2.0}* as the most effective configuration for achieving robust frequency stability and reduced dynamic errors. Additionally, tabulated data of tuning parameters and time domain specifications of model validate the FOPID control designs for frequency stability of $Dz\mu G$ model.

The proposed Bayat-driven FOPID controller design has several limitations. Its tuning is system-specific and may not generalize well to other microgrid configurations without re-tuning. The reliance on reduced-order models introduces performance sensitivity to modeling inaccuracies. While OPAL-RT real-time validation adds value, it does not fully capture physical nonlinearities or communication issues encountered in practical deployment. Moreover, the study does not explore the controller's robustness under extreme disturbances or compare it extensively with other optimization techniques. Finally, economic and cybersecurity aspects, crucial for real-world microgrid applications, remain unaddressed.

Looking ahead, future endeavors could integrate advanced control techniques to tune FOPID controllers using learning-based optimization approaches. Moreover, the cascaded based control design could be explored as an extension of this work to maintain frequency stability of the $Dz\mu G$ model. Another promising avenue for extending this work involves addressing the cybersecurity issues associated with various control strategies and enhancing the resilience of microgrids. Further, the efficacy of the FOPID controller is tested for probabilistic profiles of solar and wind power in the future.

Data availability

All data generated or analysed during this study are included in this published article.

Received: 29 May 2025; Accepted: 17 September 2025

Published online: 22 October 2025

References

- Mohammed, A., Kadry, A., Abo-Adma, M., Samahy, A. E. & Elazab, R. Continuous-time robust frequency regulation in isolated microgrids with decentralized fixed structure μ -synthesis and comparative analysis with PID and FOPID controllers. *Sci. Reports* **14**, 20800 (2024).
- Davoudkhani, I. F. et al. Maiden application of mountaineering team-based optimization algorithm optimized 1PD-PI controller for load frequency control in islanded microgrid with renewable energy sources. *Sci. Reports* **14**, 22851 (2024).
- Daraz, A. et al. Frequency stabilization of interconnected diverse power systems with integration of renewable energies and energy storage systems. *Sci. Reports* **14**, 25655 (2024).
- Bashishtha, T., Singh, V., Yadav, U. & Varshney, T. Reaction curve-assisted rule-based PID control design for islanded microgrid. *Energies* **17**, 1110 (2024).
- Daraz, A. et al. Load frequency stabilization of distinct hybrid conventional and renewable power systems incorporated with electrical vehicles and capacitive energy storage. *Sci. Reports* **14**, 9400 (2024).
- Latif, A., Hussain, S. S., Das, D. C. & Ustun, T. S. Optimization of two-stage IPD-(1+ I) controllers for frequency regulation of sustainable energy based hybrid microgrid network. *Electronics* **10**, 919 (2021).
- Faragalla, A., Abdel-Rahim, O., Orabi, M. & Abdelhameed, E. H. Enhanced virtual inertia control for microgrids with high-penetration renewables based on whale optimization. *Energies* **15**, 9254 (2022).
- Boopathi, D., Jagatheesan, K., Anand, B., Samanta, S. & Dey, N. Frequency regulation of interlinked microgrid system using mayfly algorithm-based PID controller. *Sustainability* **15**, 8829 (2023).
- Sanki, P., Mazumder, S., Basu, M., Pal, P. S. & Das, D. Moth flame optimization based fuzzy-PID controller for power-frequency balance of an islanded microgrid. *J. The Inst. Eng. (India): Ser. B* **102**, 997–1006 (2021).
- Khadanga, R. K., Padhy, S., Panda, S. & Kumar, A. Design and analysis of multi-stage PID controller for frequency control in an islanded micro-grid using a novel hybrid whale optimization-pattern search algorithm. *Int. J. Numer. Model. Electron. Networks, Devices Fields*, **31**, e2349 (2018).
- Alhejji, A., Ahmed, N., Ebeed, M., Sayed, K. & Refai, A. A robust cascaded controller for load frequency control in renewable energy integrated microgrid containing PEV. *Int. J. Renew. Energy Res. (IJRER)* **13**, 423–433 (2023).
- Khamari, D., Sahu, R. K. & Panda, S. A modified moth swarm algorithm-based hybrid fuzzy PD-PI controller for frequency regulation of distributed power generation system with electric vehicle. *J. Control. Autom. Electr. Syst.* **31**, 675–692 (2020).
- Mahakur, A. & Mohanty, D. Frequency control of SPV/wind/biogas/biodiesel-based microgrid using fuzzy-aided PID controllers. In *Sustainable Energy and Technological Advancements: Proceedings of ISSETA 2021*, 611–624 (Springer, 2022).
- Padhy, S. et al. Marine predator algorithm based PD-(1+ PI) controller for frequency regulation in multi-microgrid system. *IET Renew. Power Gener.* **16**, 2136–2151 (2022).
- Zishan, F., Akbari, E., Montoya, O. D., Giral-Ramírez, D. A. & Molina-Cabrera, A. Efficient PID control design for frequency regulation in an independent microgrid based on the hybrid PSO-GSA algorithm. *Electronics* **11**, 3886 (2022).
- Barik, A. K. & Das, D. C. Expedited frequency control of solar photovoltaic/biogas/biodiesel generator based isolated renewable microgrid using grasshopper optimisation algorithm. *IET Renew. Power Gener.* **12**, 1659–1667 (2018).
- Roy, S. P., Shubham, M., Singh, A. & Roy, O. A maiden application of an MGO-tuned cascade controller for the secondary frequency control in biogas-powered marine shipboard microgrid. *Int. J. Ambient Energy* **45**, 2402738 (2024).
- Sahu, S. N., Khadanga, R. K., Arya, Y. & Panda, S. Analysis of ultra-capacitor and plug-in electric vehicle for frequency regulation of a distributed power generation system utilizing novel modified gorilla troops optimizer algorithm. *Electr. Eng.*, 1–14 (2024).
- Ray, P. K., Mohanty, S. R. & Kishor, N. Proportional-integral controller based small-signal analysis of hybrid distributed generation systems. *Energy Convers. Manag.* **52**, 1943–1954 (2011).
- Kullapadayachi Govindaraju, S. & Sivalingam, R. Design, analysis, and real-time validation of type-2 fractional order fuzzy PID controller for energy storage-based microgrid frequency regulation. *Int. Transactions on Electr. Energy Syst.* **31**, e12766 (2021).
- Raju, G. V. & Srikanth, N. V. Frequency control of an islanded microgrid with multi-stage PID control approach using moth-flame optimization algorithm. *Electr. Eng.*, 1–18 (2024).
- Mehta, S. & Basak, P. A centralized stage-wise control approach for frequency and voltage regulation in PV–wind–storage based islanded microgrid. *Electr. Power Components Syst.*, 1–19 (2023).
- Gope, S., Reddy, G. H. & Singh, K. M. Frequency regulation analysis for renewable bio generated autonomous multi-microgrid using moth flame optimized fractional order controller. *Mater. Today: Proc.* **80**, 753–761 (2023).
- Mishra, S., Prusty, R. C. & Panda, S. Design and analysis of 2DOF-PID controller for frequency regulation of multi-microgrid using hybrid dragonfly and pattern search algorithm. *J. Control. Autom. Electr. Syst.* **31**, 813–827 (2020).
- Annamraju, A. & Nandiraju, S. Robust frequency control in an autonomous microgrid: a two-stage adaptive fuzzy approach. *Electr. Power Components Syst.* **46**, 83–94 (2018).
- Gupta, S., Mukhopadhyay, S., Banerji, A., Sanki, P. & Biswas, S. K. Student psychology-based optimization tuned PIDA controller for improved frequency regulation of a two-area microgrid. *Arab. J. for Sci. Eng.*, 1–22 (2024).
- Srinivasarathnam, C., Yammani, C. & Maheswarapu, S. Load frequency control of multi-microgrid system considering renewable energy sources using grey wolf optimization. *Smart Sci* **7**, 198–217 (2019).
- Banki, T., Faghihi, F. & Soleimani, S. Frequency control of an island microgrid using reset control method in the presence of renewable sources and parametric uncertainty. *Syst. Sci. & Control. Eng.* **8**, 500–507 (2020).
- Jabari, M. et al. A novel artificial intelligence based multistage controller for load frequency control in power systems. *Sci. Reports* **14**, 29571 (2024).
- Helaimi, M., Gabbar, H. A., Taleb, R. & Regad, M. Frequency control scheme based on the CDM-PID controller for the hybrid microgrid system with stochastic renewable generators. *Automatika* **64**, 484–495 (2023).
- Mohamed, M. A. E., Jagatheesan, K. & Anand, B. Modern PID/FOPID controllers for frequency regulation of interconnected power system by considering different cost functions. *Sci. Reports* **13**, 14084 (2023).
- Khadanga, R. K., Das, D., Kumar, A. & Panda, S. An improved parasitism predation algorithm for frequency regulation of a virtual inertia control based AC microgrid. *Energy Sources, Part A: Recover. Util. Environ. Eff.* **44**, 1660–1677 (2022).
- Shiva, C. K. et al. Forward-thinking frequency management in islanded marine microgrid utilizing heterogeneous source of generation and nonlinear control assisted by energy storage integration. *Sci. Reports* **15**, 1–33 (2025).
- Sahu, P. C., Prusty, R. C. & Panda, S. Frequency regulation of an electric vehicle-operated micro-grid under WOA-tuned fuzzy cascade controller. *Int. J. Ambient Energy* **43**, 2900–2911 (2022).
- Sekhar, P. & Mishra, S. Storage free smart energy management for frequency control in a diesel-PV-fuel cell-based hybrid AC microgrid. *IEEE Trans. Neural Netw. Learn. Syst.* **27**, 1657–1671 (2015).
- Sharma, M., Dhundhara, S., Arya, Y. & Prakash, S. Frequency stabilization in deregulated energy system using coordinated operation of fuzzy controller and redox flow battery. *Int. J. Energy Res.* **45**, 7457–7475 (2021).
- Hussain, S. & Gabbar, H. A. A multi-objective evolutionary optimization of fuzzy controller for energy conservation in air conditioning systems. *Int. J. Energy Res.* **38**, 847–859 (2014).

38. Zibandeh, H., Ghafouri, A. & Nouri, T. Innovative type II fuzzy-based voltage–frequency controller for isolated microgrid considering load shedding and uncertainties. *Int. J. Energy Res.* **2024**, 8718931 (2024).
39. Bashishttha, T. et al. ITAE index based control design strategy to mitigate frequency deviation of renewable integrated islanded-microgrid. In *2024 IEEE International Conference on Power Electronics, Drives and Energy Systems (PEDES)*, 1–5 (IEEE, 2024).
40. Bashishttha, T., Singh, V., Mathur, A. & Murari, K. PID control design using ITSE index for load frequency stability in renewable integrated standalone microgrids. In *2024 2nd International Conference on Cyber Physical Systems, Power Electronics and Electric Vehicles (ICPEEV)*, 1–5 (IEEE, 2024).
41. Bashishttha, T. et al. Efficient load frequency regulation of islanded microgrids with fractional-order PI controller. In *2024 IEEE International Conference on Power Electronics, Drives and Energy Systems (PEDES)*, 1–5 (IEEE, 2024).
42. Sahu, P. C., Mishra, S., Prusty, R. C. & Panda, S. Improved-salp swarm optimized type-II fuzzy controller in load frequency control of multi area islanded AC microgrid. *Sustain. Energy, Grids Networks*, **16**, 380–392 (2018).
43. Sahu, P. C., Prusty, R. C. & Panda, S. Improved-GWO designed FO based type-II fuzzy controller for frequency awareness of an AC microgrid under plug in electric vehicle. *J. Ambient Intell. Humaniz. Comput.* **12**, 1879–1896 (2021).
44. Sahu, P. C., Prusty, R. C. & Panda, S. Optimal design of a robust FO-multistage controller for the frequency awareness of an islanded AC microgrid under I-SCA algorithm. *Int. J. Ambient Energy* **43**, 2681–2693 (2022).
45. Sahu, P. C. & Samantaray, S. R. Resilient frequency stability of a PV/wind penetrated complex power system with CSA tuned robust type-2 fuzzy cascade PIF controller. *Electr. Power Syst. Res.* **225**, 109815 (2023).
46. Bashishttha, T. & Singh, V. Chien-Hrones-Reswick method-based PID control strategy for mitigation of frequency deviation of islanded microgrid. *Electr. Eng.*, 1–15 (2025).
47. Prusty, U. C., Nayak, P. C., Prusty, R. C. & Panda, S. An improved moth swarm algorithm based fractional order type-2 fuzzy PID controller for frequency regulation of microgrid system. *Energy Sources, Part A: Recover. Util. Environ. Eff.*, 1–23 (2022).
48. Mishra, D., Sahu, P. C., Prusty, R. C. & Panda, S. A fuzzy adaptive fractional order-PID controller for frequency control of an islanded microgrid under stochastic wind/solar uncertainties. *Int. J. Ambient Energy* **43**, 4602–4611 (2022).
49. Merrikh-Bayat, F. General rules for optimal tuning the $PI^{\lambda}D^{\mu}$ controllers with application to first-order plus time delay processes. *The Can. J. Chem. Eng.* **90**, 1400–1410 (2012).
50. Sánchez, H. S., Padula, F., Visioli, A. & Vilanova, R. Tuning rules for robust FOPID controllers based on multi-objective optimization with FOPDT models. *ISA Transactions* **66**, 344–361 (2017).
51. Merrikh-Bayat, F. Optimal tuning rules of the fractional-order PID controllers with application to first-order plus time delay processes. In *2011 International Symposium on Advanced Control of Industrial Processes (ADCONIP)*, 403–408 (IEEE, 2011).
52. Vinagre, B., Podlubny, I., Hernandez, A. & Feliu, V. Some approximations of fractional order operators used in control theory and applications. *Fract. Calculus Appl. Anal.* **3**, 231–248 (2000).
53. Tricaud, C. & Chen, Y. An approximate method for numerically solving fractional order optimal control problems of general form. *Comput. Math. with Appl.* **59**, 1644–1655 (2010).

Author contributions

Conceptualization, T. K. B., V. P. S., T. V.; methodology, T. K. B., V. P. S.; software, T. K. B.; validation, T. K. B., V. P. S., T. V.; formal analysis, T. K. B., V. P. S., S. P.; investigation, T. K. B., V. P. S.; resources, T. K. B., V. P. S., T. V., S. P.; data curation, T. K. B., V. P. S.; writing—original draft preparation, T. K. B.; writing—review and editing, T. K. B., V. P. S., Funding, S. P.

Funding

Open access funding provided by University Of South-Eastern Norway. The authors did not receive funding from any organization for the submitted work.

Declarations

Consent for publication

All authors have read and agreed to the published version of the manuscript.

Competing interests

The authors declare no competing interests.

Additional information

Correspondence and requests for materials should be addressed to S.P.

Reprints and permissions information is available at www.nature.com/reprints.

Publisher's note Springer Nature remains neutral with regard to jurisdictional claims in published maps and institutional affiliations.

Open Access This article is licensed under a Creative Commons Attribution 4.0 International License, which permits use, sharing, adaptation, distribution and reproduction in any medium or format, as long as you give appropriate credit to the original author(s) and the source, provide a link to the Creative Commons licence, and indicate if changes were made. The images or other third party material in this article are included in the article's Creative Commons licence, unless indicated otherwise in a credit line to the material. If material is not included in the article's Creative Commons licence and your intended use is not permitted by statutory regulation or exceeds the permitted use, you will need to obtain permission directly from the copyright holder. To view a copy of this licence, visit <http://creativecommons.org/licenses/by/4.0/>.

© The Author(s) 2025